Moazen Dehkordi, Shokouh

Material Modelling for Gas Manifolds in Marine Engines

School of Technology and Innovations
Master's thesis in Industrial
Systems Analytics

Vaasa 2026

UNIVERSITY OF VAASA
School of Technology and Innovations

Author:	Moazen Dehkordi, Shokouh
Title of the Thesis:	Material Modelling for Gas Manifolds in Marine Engines
Degree:	Master’s
Programme:	Industrial Systems Analytics
Supervisor:	Dr. Ahm Shamsuzzoha, Dr. Arturo Rubio Ruiz
Year:	2026 **Sivumäärä:** 82

ABSTRACT :

AISI 316L stainless steel is a popular choice for marine engine parts because of its excellent resistance to corrosion, good weldability, and reliable mechanical performance. However, this steel undergoes complex cyclic plastic deformation under repeated loading, including nonlinear hardening, cyclic stabilization, and strain-amplitude-dependent hardening, which are challenging features for constitutive modelling. These effects are not properly captured by simplified constitutive models that are typically employed in industrial finite element analyses, e.g., elastic-perfect plastic formulation. Therefore, the estimation of local stresses, plastic strains and fatigue-critical areas might not be trustworthy. This thesis is mainly aimed at enhancing the constitutive modelling capability of cyclic plasticity of AISI 316L stainless steel and investigating the impact of sophisticated material modelling on the predicted response of marine engine gas manifold components. More specifically, the work explores whether a constitutive model with nonlinear kinematic hardening, isotropic hardening, viscoplasticity, and strain-amplitude-dependent hardening can reproduce the experimentally observed cyclic behavior of AISI 316L and provide finite element predictions that are more accurate and credible than simple material models. A one-dimensional implementation for the chosen constitutive model was created and tested versus a simple example from the Z-set materials library. The cyclic loading experiments that had been performed and published were digitized, analyzed, and used for parameter identification. To calibrate the model, a combination of global and local optimization methods was used to fit the parameters to the stress-strain hysteresis loops and the evolution of peak stress data. The trained model was later tested on different experimental cases that were not part of the training set. The parameterized constitutive model was able to match the cyclic hardening, hysteresis loop development, and stress stabilization data for different strain levels obtained from the experiments. In addition, the parameters related to isotropic hardening and memory effects were varied to study their impact on the cyclic response. At last, the calibrated material model was integrated into an Abaqus finite element submodel of a marine engine gas manifold. The findings revealed major changes in local stress redistribution, stress concentration phenomenon, and plastic strain evolution as compared to the traditional elastic-perfect plastic material model. The research indicates that the advanced material modelling of cyclic plasticity, an AISI 316L behavior representation could be achieved that is closer to reality and therefore enhance the prediction of mechanical weak points in marine engine structures. This modelling approach, therefore, constitutes a practicable method for engineering analyses requiring both high fidelity of prediction and numerical robustness.

KEYWORDS: Cyclic Plasticity/AISI 316L Stainless Steel/Constitutive material modelling/Kinematic Hardening/Isotropic Hardening/Strain amplitude dependent hardening/Viscoplasticity

Contents

Pictures

No table of figures entries found.

Figures

Tables

Abbreviations

1 Introduction

1.1 Background

Marine engines are typically exposed to severe thermo-mechanical loadings involving pressure fluctuations, thermal gradients, vibrations, and mechanical cyclic loadings. Such conditions can cause changes in the material structure and properties of the components leading to plastic strain, stress redistribution and damage due to fatigue for main parts of the engine (Dowling, 2013; Fatemi, 1998; Socie & Marquis, 2000; Stephens et al., 2001). Gas manifold systems, as one of these parts, are always under combined thermal and mechanical loadings. Therefore, their structural integrity depends heavily on the accurate prediction of local stress and strain distributions.

The finite element method (FEM) is widely used as a tool for studying the structural behavior of engineering components under pressure. In addition, constitutive modelling is the first step that strongly influences the performance of the finite-element model whenever the matter comes to nonlinear analysis (Lemaitre & Chaboche, 2012a). Simplified constitutive descriptions may fail to reproduce the complex cyclic deformation mechanisms resulting in an inaccurate evolution of stress, accumulation of plastic strains and misprediction of fatigue critical locations.

AISI 316L stainless steel is a low-carbon austenitic stainless steel and is known as a steel to be highly corrosion resistant, and it has excellent weldability and a wide range of good mechanical properties. For these reasons, it has been extensively used in the marine, chemical, power, and process industries (*ASM Handbook:P Roperties and Selection: Iron, Steels, and High-Performance Alloys*, 1990; Davis, 1994). Compared with regular carbon steels, AISI 316L has superior resistance to degradation by chloride-containing environments and elevated temperatures, making it an ideal material especially for gas handling systems and marine engine components (Kovach & Redmond, 2009). Therefore, AISI 316L stands as a leading candidate among materials used for gas manifolds, piping systems, pressure vessels, and other pressure containing components exposed to service conditions that are chemically aggressive.

The cyclic deformation behavior of AISI 316L is challenging and comprises different hardening mechanisms during strain reversal and results in gradual evolution of cyclic stresses with the number of cycles (Pelegatti et al., 2021; Pham et al., 2013a; Polák et al., 1994; Zhou et al., 2018a). These phenomena highlight the fact that the mechanical response of the material is dependent not only on the present stress and strain state but also on the previous loading history.

1.2 Research Problem and Motivation

The main problem of this study is to accurately predict cyclic plasticity which is still a very difficult task in computational solid mechanics. Elastic-perfect plastic models are widely used in industrial finite element analyses since they are often simply adopted in industrial analyses and can represent some aspects of mechanical behaviour. However, they cannot represent the description of most of the physical behaviours observed in experiments, such as cyclic hardening, cyclic softening, stress stabilization, the Bauschinger effect, and strain-amplitude-dependent hardening (Armstrong & Federick, 1966; Chaboche, 1989; Jiang & Sehitoglu, 1996).

Because of the need for a quantitative understanding of the effects of repetitive cyclic loading, constitutive equations based on nonlinear kinematic hardening and isotropic hardening have been developed. Among these approaches, the Chaboche constitutive model has become one of the most widely used formulations for cyclic plasticity simulations because of its ability to reproduce complex cyclic material behaviour while maintaining computational efficiency (Chaboche, 1989, 2008).

Besides, various research works found the cyclic behaviour of AISI 316L to be quite heavily dependent on strain amplitudes as well as loading sequences (Pham et al., 2013a; Polak & Man, 2016). To really describe constitutive behaviour with high fidelity, nonlinear hardening effects together with the ability of the material to remember previous deformation histories must be considered.

From an engineering viewpoint, this problem is extremely relevant in the case of gas manifolds. Different sections of the manifold may be exposed to very different local strain amplitudes during service, which would result in different hardening states and levels of stress. Therefore, the use of overly simplified constitutive models may yield non-physical stress results and lead to wrong conclusions about structural integrity.

Extensive research has been conducted on the cyclic plasticity characteristics of AISI 316L stainless steel. These investigations revealed the criticality of nonlinear kinematic hardening, isotropic hardening, and memory effects to account for the experimentally observed response accurately (Pham et al., 2013a; Polák et al., 1994; Zhou et al., 2018a). Likewise, constitutive models that can describe such behaviour were first introduced decades ago and have evolved since then (Chaboche, 1989, 2008).

However, there has been very little research done on the systematic parametrization of strain-amplitude-dependent constitutive models of AISI 316L based on published cyclic experimental tests. Furthermore, there are not enough documented studies examining the effect of implemented advanced cyclic plasticity models on the resulting stress and strain fields in components of gas manifolds. This disparity in literature forms the basis of the motivation for the present paper.

1.3 Research Questions

This thesis attempts to answer the following research questions:

RQ1: Is it possible for a constitutive model that includes nonlinear kinematic hardening, isotropic hardening, viscoplasticity, and strain-amplitude-dependent hardening to correctly reproduce the cyclic behaviour of AISI 316L stainless steel?

RQ2: Can the set-up model estimate cyclic responses at strain amplitudes that are different from those used during calibration?

RQ3: What effects does using a sophisticated constitutive model have on the finite element gas manifold analysis stress and strain predictions when compared to a simple elastic-perfectly plastic material model?

1.4 Research Objectives

This research aims at:

- Developing and implementing a constitutive framework that can capture the phenomena of cyclic hardening and strain-amplitude-dependent behaviour.
- Using cyclic loading data obtained from experiments reported in the literature as a basis for parameter identification of the model.
- Carrying out the validation of the calibrated model for predicting new loading scenarios.
- Examining the role of material parameters in the cyclic loading performance.
- Utilizing the established model in a finite element submodel of a gas manifold, followed by the assessment of changes in structural response predictions.

1.5 Structure of the Thesis

This thesis is divided into a number of chapters that cover the following topics:

Chapter 2 reviews previous work on cyclic plasticity, constitutive modelling, memory effects, and the cyclic behaviour of AISI 316L stainless steel.

Chapter 3 elaborates on the technique of model implementation, parameter calibration, and validation.

Chapter 4 deals with the presenting of model verification, calibration, validation, and first application results to the gas manifold submodel.

In chapter 5, the discussion mainly revolves around the interpretation of the findings obtained. It also includes a comparison of the advanced constitutive model to the basic one and describes the study limitations as well as the engineering significance.

To conclude, Chapter 6 reviews the main points of the study and offers suggestions for future work.

2 Literature review

This chapter reviews all relevant published work on the cyclic plastic behaviour of metal materials, mainly on AISI 316L stainless steel. First, a brief note is made on why accurate material modelling is crucial from an engineering perspective. Then, the normal cyclic plasticity constitutive modelling approaches, such as isotropic hardening, kinematic hardening, viscoplasticity, and strain-amplitude-dependent hardening are briefly explained. Lastly, a review is made of the issues and drawbacks of the presently existing models and the research gap filled by this thesis is revealed.

2.1 Cyclic behavior of AISI 316L Stainless STEEL

AISI 316L is one of the main austenitic stainless steel with low carbon that has a wide commercial use in marine, chemical, power and processing industries owing to the combination of very high corrosion resistance, produce easily welding and the perfect combination of strength and ductility (*ASM Handbook:P Roperties and Selection: Iron, Steels, and High-Performance Alloys*, 1990; Davis, 1994; Sedriks, 1996). Besides that, the incorporation of molybdenum promotes resistance against localized corrosion, especially in chloride environments which have made AISI 316L as a material of choice for components subjected to operating service under quite aggressive conditions. Consequently, the product is being widely used in piping systems, pressure-containing components, heat exchangers, and marine-engine assemblies where not only mechanical performance but also corrosion resistance is required.

In comparison with traditional carbon steels, AISI 316L has higher corrosion resistance and ductility, yet the way it deforms under cyclic loading is much more complicated (Lippold & Damian, 2005). Cyclic behavior results from the changes in the dislocation structures and internal stresses that are generated during the process of loading and unloading being repeated. On top of that, the material may show nonlinear hardening behavior, evolution of hysteresis loops, and dependence on loading history which are features that simple elastic-perfectly plastic constitutive models cannot deal with adequately (Chaboche, 2008; Mughrabi, 2002; Polak & Man, 2016).

Experimental investigations have shown that the cyclic behavior of AISI 316L is highly dependent on the applied strain amplitude. When subjected to cyclic loading, the material usually first shows cyclic hardening during the first few cycles and then the stress response stabilizes slowly. Also, different strain amplitudes can cause significantly different stress levels and hardening rates after stabilization, which means that material response depends not only on the current deformation state but also on the previous loading history (Pham et al., 2013a; Polak & Man, 2016). Such strain-amplitude-dependent behavior presents a challenge for constitutive modeling and parameter identification.

Many authors have found that standard cyclic plasticity models frequently fail to accurately describe the experimentally observed hardening evolution of AISI 316L under different strain amplitudes. Literature proposes to use advanced constitutive models designed with nonlinear kinematic hardening, isotropic hardening, and memory effects (Abdel-Karim & Ohno, 2000; Chaboche, 1989; Jiang & Sehitoglu, 1996). By these methods, the material model can simulate the loading-history effects and strain-amplitude-dependent hardening.

The goal of this study is to implement and calibrate a constitutive model that can reproduce the cyclic behaviors of AISI 316L stainless steel accurately. Therefore, it is crucial to have a thorough understanding of the cyclic behavior of the material as observed in experiments. For this purpose, the next sections first review the constitutive modelling methods that are frequently used to characterize cyclic plasticity and material behavior that depends on loading history.

2.2 Engineering context and the need for reliable material modelling

Mechanical design and the analysis of structural performance rely heavily on the correct prediction of finite element simulations, which in turn depends on the selection of an accurate material constitutive model. Simplified material models are commonly used, but they might not adequately describe the behavior of materials subjected to repeated plastic deformation. As a result, inaccurate estimation of stresses and strains can hinder fatigue and durability assessments.

AISI 316L shows a complex cyclic response that cannot be described adequately by simplified constitutive assumptions. Experimental evidence shows that this material exhibits strain amplitude dependent hardening and a non-monotonic hardening trend during strain-controlled cyclic loading (Pelegatti et al., 2021; Pham et al., 2013a; Zhou et al., 2018). Figure 1 shows the evolution of the cycle peak stress evolution of AISI 316L at different strain amplitudes measured by Pelegatti et al (2021). Zhou et al. (2018b) demonstrated that different loading paths can result in long softening regimes that are followed by rehardening, while Polák et al.(1994) showed that the cyclic response of 316L is complex and cannot be represented by one single universal curve but rather consists of several behavioral domains depending on the deformation level.

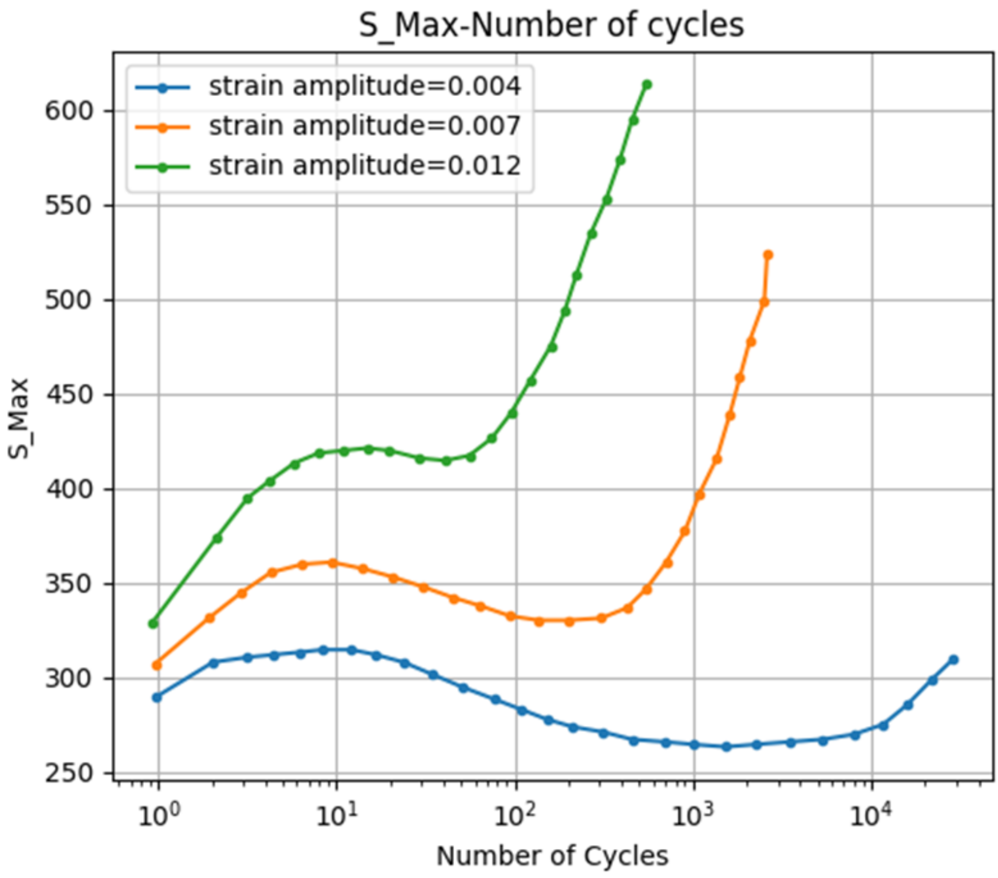

Figure 1 Peak stress evolution during cyclic strain-controlled tension-compression of 316L (Pelegatti et al., 2021).

2.3 Challenges in representing Cyclic Material Behavior

One of the main challenges in modelling cyclic deformation relates to the fact that the material response is not controlled solely by the current stress or strain level but is also influenced by the loading history (Krempl, 2001; McDowell, 1995). As mentioned in section 2.1, a particular aspect of 316L in cyclic loadings is that it exhibits strain amplitude dependent hardening, which means that different cycle strain amplitudes lead to different hardening levels. This feature is relevant for gas manifolds, where different locations can experience different strain amplitudes under cyclic loading and therefore different stress levels would be developed.

2.4 Cyclic plasticity modelling

The numerical description of cyclic plasticity requires the use of internal variables responsible for tracking hardening and accumulated strain (Chaboche, 1989, 2008). The stress space is typically divided into elastic and plastic regions. The elastic part obeys Hooke’s law whereas plastic deformation depends on plasticity related features explained here after.

One aspect of plastic deformation cyclicity is the modeling of hysteresis loops, cyclic hardening and softening, and ratcheting in metals. The unified viscoplastic constitutive models proposed by Chaboche stand out as the most popular ones among the numerous existing formulations since they involve the combination of isotropic hardening, kinematic hardening, and rate-dependent plastic flow in one model (Chaboche, 1989, 2008). The implementation of these models has shown good results for stainless steels, structural steels, and high-temperature alloys under cyclic loading (Besson et al., 2009).

2.4.1 Strain Decomposition and Elastic Response

The constitutive framework used in this study is based on the elasto-viscoplastic formulation reported by Chaboche (1989) and enriched with the work of Lemaitre and Chaboche for strain amplitude dependence (Chaboche, 1989, 1989; Lemaitre & Chaboche, 2012b).

The idea of breaking down the total strain into elastic and plastic parts is the starting point of classical elastoplasticity theory. It is based on the assumption that one can distinguish between the reversible elastic deformation and the irreversible plastic deformation that is accumulated during the loading process. This kind of splitting has been the most common feature of the constitutive formulations because it gives a physically meaningful basis for explaining cyclic deformation and the development of internal state variables (Lemaitre & Chaboche, 2012b; Simo & Hughes, 1998).

The total strain is formed of elastic and plastic parts (Dunne & Petrinic, 2005):

$$\varepsilon = \varepsilon^{e} + \varepsilon^{pl} \tag{1}$$

The stress–strain relationship is controlled by linear elasticity (Simo & Hughes, 1998):

$$\sigma = C : (\varepsilon - \varepsilon^{pl}) \tag{2}$$

where C is the fourth-order elasticity tensor.

The elastic constitutive relation determines the stress response when the material is still inside the yield surface. After the yield condition is achieved, the excess plastic strain arises, and the material response is then governed by the hardening laws and visco-plastic flow rules explained in the next sections (Dunne & Petrinic, 2005).

2.4.2 Yield Function and Internal Variables

One of the ways to determine when a material is changing from elastic behaviour to plastic one is through a yield criterion. Yielding usually happens in metallic materials when irreversible dislocation motion is activated. Since ductile metals after yielding are typically controlled by their deviatoric stress state and not hydrostatic pressure, the von Mises criterion is widely used (Mises, 1913). When the material is cyclically deformed, the yield surface will be changing all the time as a result of isotropic and kinematic hardening processes that are described by internal variables (Chaboche, 2008; Hill, 1950). Plastic deformation starts when the stress state reaches the yield surface. The yield surface defines the boundary between elastic and plastic behavior in space. Therefore, the yield criteria are written as (Mises, 1913):

$$f(\sigma) \begin{cases} <0 & \text{elastic region} \\ >0 & \text{viscoplastic region} \end{cases} \tag{3}$$

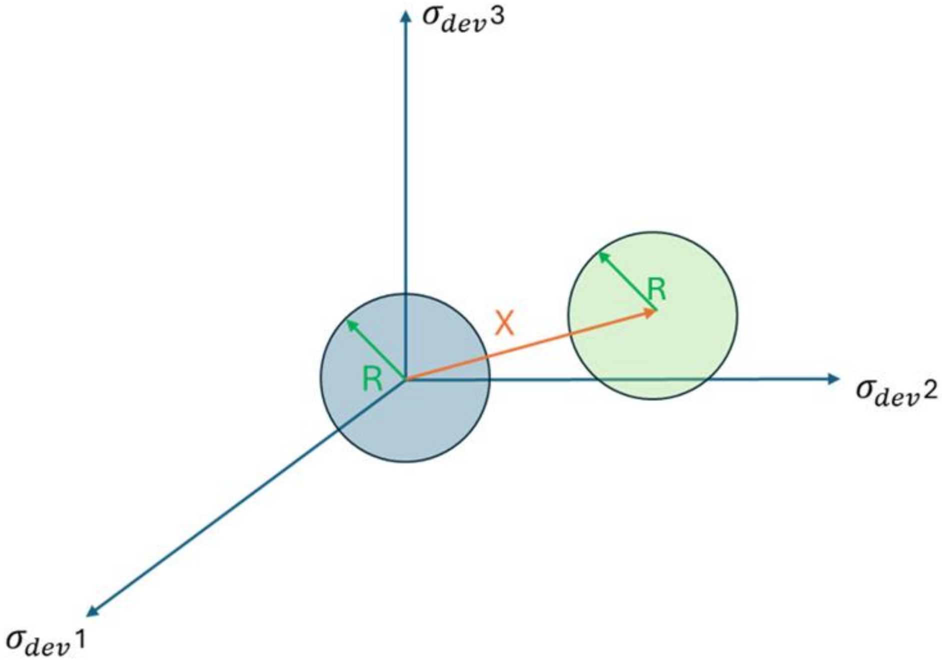

Figure 2 Geometrical representation of the yield surface (adapted from Lemaitre & Chaboche (2012))

In the Chaboche framework, the backstress tensor X controls the position of the yield surface, while its size is controlled by the isotropic hardening variable R. For describing cyclic plasticity, both kinematic and isotropic hardening mechanisms are implemented. The yield function is defined as (Chaboche, 1989):

$$f(\sigma, X, R) = J(\sigma - X) - (\sigma_{y0} + R) \tag{4}$$

where:

X is the total backstress tensor

R is the isotropic hardening variable.

σ_{y0} is the initial yield stress.

$J\,(\cdot)$ shows the von Mises equivalent stress.

2.4.3 Nonlinear Kinematic Hardening (Chaboche Model)

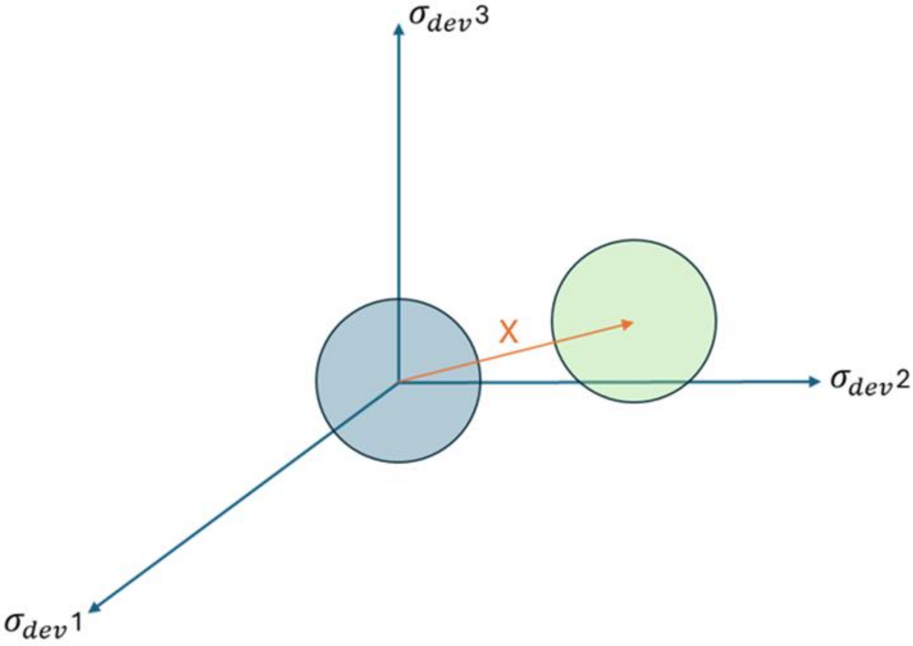

Figure 3 Schematic of Kinematic Hardening and translation of the yield surface (adapted from Lemaitre and Chaboche (2012))

Kinematic hardening is a concept that tries to explain the movement of the yield surface in the stress space when a material undergoes cyclic loading. The main reason for introducing kinematic hardening is to model the Bauschinger effect, which is a phenomenon where the yield stress is reduced after the load reversal due to the internal stress fields caused by the dislocation structures. The nonlinear Armstrong-Frederick model and its generalization by Chaboche have become very popular as they very well capture the short-term cyclic hardening and hysteresis loop changes (Armstrong & Federick, 1966; Chaboche, 1989; Ohno & Wang, 1993). By using kinematic hardening, the yield surface is shifted which is required to model the Bauschinger effect (Chaboche, 1989, 2008). The overall backstress tensor is the result of the addition of multiple components X_i (Armstrong & Federick, 1966)

$$X = \sum_{i=1}^{2} X_i \tag{5}$$

Each backstress component is representative for a different kinematic hardening with its own evolution rate. The change of every backstress component is controlled by the non-linear kinematic hardening rule suggested by Chaboche in equation 6 (Armstrong & Federick, 1966):

$$Xi = (⅔)C_i(n - (3D_i/2C_i)X_i)\dot{p} \tag{6}$$

C_i shows the kinematic hardening modulus.
D_i is the dynamic recovery parameter.
$\dot{p}$ is the equivalent plastic strain rate.
Allowing the model to have several backstress components is equivalent to having multiple hardening mechanisms that work at different speeds. As a result, it is possible to simulate the short-term as well as the long-term cyclic behaviors in a much more faithful way.

2.4.4 Isotropic Hardening (Voce Law)

Unlike kinematic hardening, isotropic hardening controls the change in size of the yield surface. From a physical point of view, isotropic hardening corresponds to the build-up of dislocations and the formation of microstructural defects that result in the material becoming more resistant to plastic deformation. Due to its simplicity and effectiveness, the Voce hardening law is widely used to fit the experimental results of metals that show a saturation in their response (Chaboche, 2008; Voce, 1948).

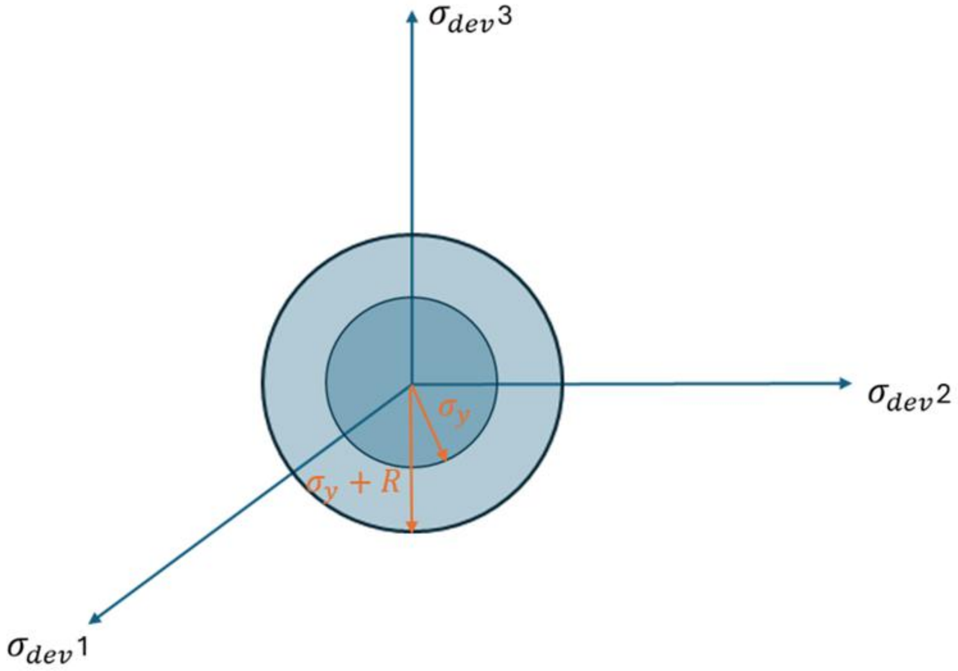

Figure 4 Schematic of Isotropic Hardening and expansion of the yield surface (adapted from Lemaitre and Chaboche(2012b))

The isotropic hardening is controlled by a variable R controlling the radius of the yield function (Chaboche, 1989, 2008) and is introduced as the result of the sum of multiple components as shown in equation 7, each of them with evolution given by equation 8(Voce, 1948).

$$R = \sum_{i=1}^{2} R_i \tag{7}$$

The behavior of isotropic hardening is described by using a multi-component Voce-type law (Chaboche, 1989):

$$(\dot{R_i}) = b_i\left(Q_{sat,i} - R_i\right) \dot{p} \tag{8}$$

$Q_{sat,i}$ is the saturation value that the i_{th}component of the isotropic hardening, and b_i is a parameter controlling how fast R_i approaches $Q_{sat,i}$.

The sum of isotropic hardening components makes it possible to simulate non-monotonic stress evolution during cyclic loading. Such formulations have also worked well for understanding how austenitic stainless steels behave under cyclic loading (Facheris & Janssens, 2014).

When the stress state hits the yield surface; it is needed to use a flow rule to figure out the path of the plastic strain evolution. Viscoplastic models are widespread since these formulations make it possible to work numerically in a very stable way and permit the consideration of strain rate changes. In fact, in these models, the rate at which plastic strain changes is a function of how much the stress exceeds the yield surface (Chaboche, 1989; Perzyna, 1966).

2.4.5 Flow rule

The evolution of the plastic strain in the model follows from a Norton potential yielding a plastic strain rate given by equation 9 (Chaboche, 1989).

The equivalent plastic strain rate is (Chaboche, 1989):

$$\dot{p} = \left(\frac{\langle f \rangle}{K}\right)^n \tag{9}$$

where:

K is the consistency parameter.

n is the rate sensitivity exponent.

$\langle \cdot \rangle$ stands for the Macaulay bracket.

The Norton potential includes two material parameters that determine how a material's deformation rate influences its properties. With larger exponents, the material's behaviour will more resemble that of a rate-independent plasticity, while smaller values generate greater loading rates which will affect the material response.

2.4.6 Limitation of the original Chaboche–Voce Model

Many constitutive models have been developed to describe cyclic plasticity in metallic materials. The original Chaboche–Voce framework that combines isotropic and kinematic hardening can reproduce key features of cyclic plasticity behavior, including stress-strain hysteresis loop evolution and cycle stabilization(Chaboche, 1989, 2008; Frederick & Armstrong, 2007). However, it assumes a monotonic evolution of the iso-tropic hardening variable toward a single saturation value (Chaboche, 1989). As a result, the model cannot represent strain-amplitude-dependent hardening, which is a relevant phenomenon in the plastic flow of AISI 316L (Pelegatti et al., 2021; Pham et al., 2013b; Zhou et al., 2018a). Therefore, an additional history-dependent mechanism is required to account for the influence of loading history on cyclic hardening.

2.4.7 Strain amplitude dependent hardening

The alloy AISI 316L exhibits strain amplitude dependent hardening is a critical challenge. Cyclic responses and the evolution of hysteresis loops could be captured by conventional kinematic hardening formulations, including multi-component Chaboche models. However, the effect of each component of backstress keeps on decreasing with the progress of cyclic loading due to the inclusion of dynamic recovery terms. As a result, these models usually fail to retain a persistent memory of maximum strain ranges experienced previously, especially after load path changes or amplitude variations. This shortcoming becomes more evident in cases with variable amplitude loading scenarios where the stabilized cyclic response is strongly affected by previous loading history. Therefore, it is necessary to incorporate additional internal variables or memory sur-face that can track the maximum strain range the material has experienced and to control the evolution of isotropic hardening. Such modifications allow the constitutive model to reproduce strain-range dependent saturation behavior and improve the pre-diction of cyclic response under complicated loading histories (Abdel-Karim & Ohno, 2000; Bari & Hassan, 2000; Ohno, 1982).

To address this issue, a strain-range memory feature is added to the constitutive model, in accordance with the concept of Chaboche (1989, 2008).

In terms of plastic strain, the strain amplitude dependent hardening is described by a memory surface:

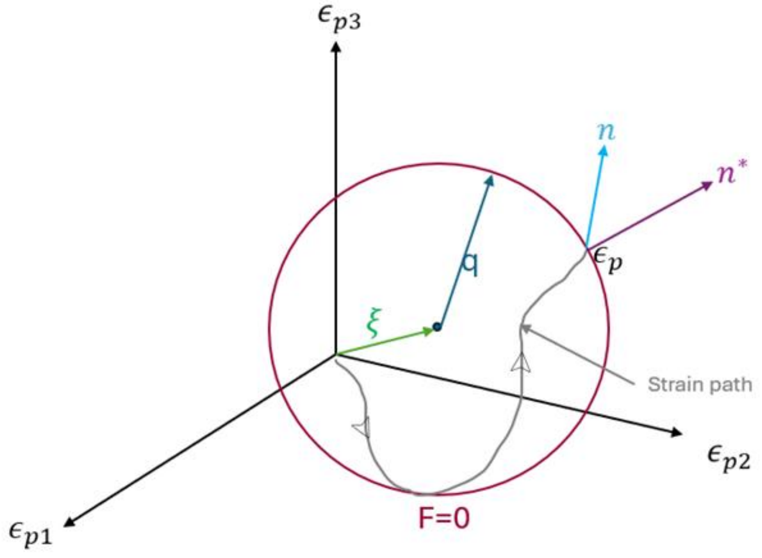

Figure 5 Geometrical representation of memory in strain surface (adapted from Z-Set Material Model Manual: Memory Behavior, n.d.)

$$F = \sqrt{(2/3)}J(\dot{p} - \xi) - q \leq 0 \tag{10}$$

where ξ is the center and q is the radius of the strain envelope surface (Chaboche, 1989). As long as the plastic strain evolves within memory surface domain $F < 0$, the memory variables do not change. Change of memory variables occurs after boundary of memory surface reaches ($F = 0$), and the loading path is forced to extend it.

The evolution equations are given as (Z-Set Material Model Manual: Memory Behavior, n.d.):

$$\xi=1/2\ (n^{*}:p)\ n^{*}\ \mathrm{H(F)} \tag{11}$$

$$\dot{q} = \eta\, \dot{p}\, H(F) \tag{12}$$

Where $H(x) = 1$ if $x > 0, H(x) = 0$ if $x < 0$. The variable η is determined by the condition of $dF = 0$ as below (Z-Set Material Model Manual: Memory Behavior, n.d.):

$$\eta = \frac{n : n*}{2|n : n*|} \tag{13}$$

Where $n^{*}$is the normal of the surface $F = 0$

$$n^{*} = \sqrt{\frac{3}{2}}\,\frac{\dot{p} - \xi}{|\dot{p} - \xi|} \tag{14}$$

These variables enable tracking of the plastic strain range. The strain amplitude de-pendent hardening is linked to isotropic hardening by means of a variable saturation level (Z-Set Material Model Manual: Memory Behavior, n.d.):

$$Q_{e}ff = Q_{sat} - (Q_{sat} - Q_{0})\exp(-2\mu q) \tag{15}$$

This formulation makes the hardening limit depend on the loading history. Therefore, the model can show different stabilized cyclic responses as a function of the strain amplitudes experienced previously (Chaboche, 1989, 2008).

2.5 Research gap and motivation

The literature indicates that the cyclic performance of AISI 316L stainless steel heavily relies on strain amplitude and loading history. It has been pointed out by experiments that cyclic hardening, cyclic softening, re-hardening, stress stabilization, and non-monotonic peak stress evolution can be observed in the material under strain-controlled cyclic loading (Pelegatti et al., 2021; Pham et al., 2013b; Polák et al., 1994; Zhou et al., 2018). This points to the fact that the material behavior is not simply represented with just one stabilized stress–strain curve or an elastic–perfectly plastic material description. To mitigate this, advanced constitutive models have been proposed with the Chaboche framework being a leading example. These models are capable of capturing key cyclic plasticity features like nonlinear kinematic hardening, isotropic hardening, the Bauschinger effect, and viscoplastic flow (Armstrong & Federick, 1966; Chaboche, 1989; Lemaitre & Chaboche, 2012). Moreover, by applying memory variables or strain-range-dependent saturation levels to such models, it becomes possible to reflect changes in hardening behavior based on strain amplitude and account for loading-history effects. Consequently, the theoretical basis that is necessary for explaining the cyclic behavior of AISI 316L can be found in the literature.

However, although these constitutive models and cyclic experimental datasets are present, their use for systematic calibration and validation of a strain-amplitude-dependent Chaboche-type model for AISI 316L is rather sparse. Using experimental data from literature could be a starting point for the identification of a model capable of not only reproducing the stress–strain hysteresis loops but also the cycle-by-cycle evolution of the maximum stress. In addition, the role of strain-amplitude-dependent hardening parameters and isotropic hardening saturation levels in controlling the predicted cyclic response have not been made clear enough for their practical use in model calibration. Therefore, from the engineering point of view, such an issue is quite relevant since the manifold gas parts of marine engines go through the effect of combined thermal, pressure, and mechanical loading. As different local regions of a manifold may go through different strain amplitudes, they will also have different cyclic hardening states. Therefore, if a simplified material model is employed, then the predicted local stress redistribution, plastic strain accumulation, and critical regions might not be representative of the real material behavior in the production setting.

The current study addresses this gap by first implementing a one-dimensional version of a strain-amplitude-dependent constitutive model and then verifying it through a Z-set reference model before parameterizing it with published cyclic experimental data for AISI 316L and finally testing the calibrated model to see if it can replicate unseen strain amplitudes. In addition, the gas manifold submodel built by finite element method is used to showcase the importance of the choice of constitutive material model on the resulting local stress and strain predictions, using the calibrated model.

3 Methodology

3.1 Overview of Methodology

The aim of this study is to calibrate the model described in the background section (Pelegatti et al., 2021), which is already available in commercial codes such as Z-mat, using relevant experimental data from the literature to improve the predictions of the mechanical response of AISI 316L under cyclic loading. From an engineering point of view, modeling cycle-by-cycle changes in the material is both impractical and unnecessary. What matters is obtaining a stabilized and representative cyclic response that captures the overall material behavior.

The constitutive formulations of section 2.3 were implemented in a one-dimensional simplification and used for calibration of the model. Before obtaining the parameters, the model was validated against the results of an example in the Z-mat library. Consequently, existing published cyclic experimental data for AISI 316L were digitized and utilized for the identification of parameters. The parameters of the model were determined through a calibration process based on optimization, and after that, they were used to predict the mechanical response of the material under unseen conditions for validation.

3.2 Modelling Assumptions and Physical Scope

While the material's response changes with each cycle, from an engineering point of view, it's not feasible or necessary to give a unique response to each load cycle. Therefore, the goal in the current modelling approach is to implement a constitutive model that is physically meaningful and can provide a representative cyclic response.

3.3 Verification of strain amplitude dependent hardening Implementation

The 1D implementation of the constitutive model is against the example case in the Z-set manual (Z-Set Material Model Manual: Memory Behavior, n.d.). The reference case uses:

- Two kinematic hardening components
- One isotropic hardening component
- Norton flow rule
- Two strain amplitude dependent hardening variables

The parameters of the reference material model are directly taken from the Z-set model manual according to table 1 to provide an equivalent comparison (Z-Set Material Model Manual: Memory Behavior, n.d.). The results of this comparison are discussed in the next chapter in section 4.1.

Table 1 The values of the parameters according to Z-set example (Z-Set Material Model Manual: Memory Behavior, n.d.)

Parameter	Value
n	7
k	100
C1	30000
C2	100000
D1	80
D2	1200
b1	25
b2	25
Q01	25
Q02	25
Qsat1	400

Qsat2	400
mu1	50
mu2	300
R0	50

3.4 Experimental data processing and preparation

3.4.1 Source of experimental data

The experimental data used in this research are obtained from the work of Pelegatti et al. (2021), who studied the cyclic behavior of AISI 316L stainless steel material under strain-controlled loading.

Two strain amplitudes are used during the calibration, 0.5 and 0.7% and the experimental data extracted for each loading condition is:

- Stress–strain hysteresis loops at certain cycles (1, 10)
- Maximum stress evolution over the cycle number (S-max vs N plots)

However, the data is not accessible in a numerical format and is only graphical, therefore a step of data digitization was required.

3.4.2 Data digitization

To make a quantitative comparison with the numerical model, the experimental data obtained were digitized from the graphs available in the literature. Each strain amplitude digitization was carried out separately to keep the amplitude-dependent characteristics of the material response. The approach includes:

- importing the graphical data into a digitizer (*WebPlotDigitizer*, n.d.).
- Selecting points on the curves.
- Transforming the extracted coordinates into numeric data sets.

Figures 6 and 7 illustrate the extracted data for both strain amplitudes ($\epsilon_a = 0.5\%, 0.7\%$) including stress-strain hysteresis loops and peak stress evolution during 10 cycles. The hysteresis loops shown in this plot are just for the first cycle at each strain amplitude, while the other cycles are also extracted and the data is shown in figure 8.

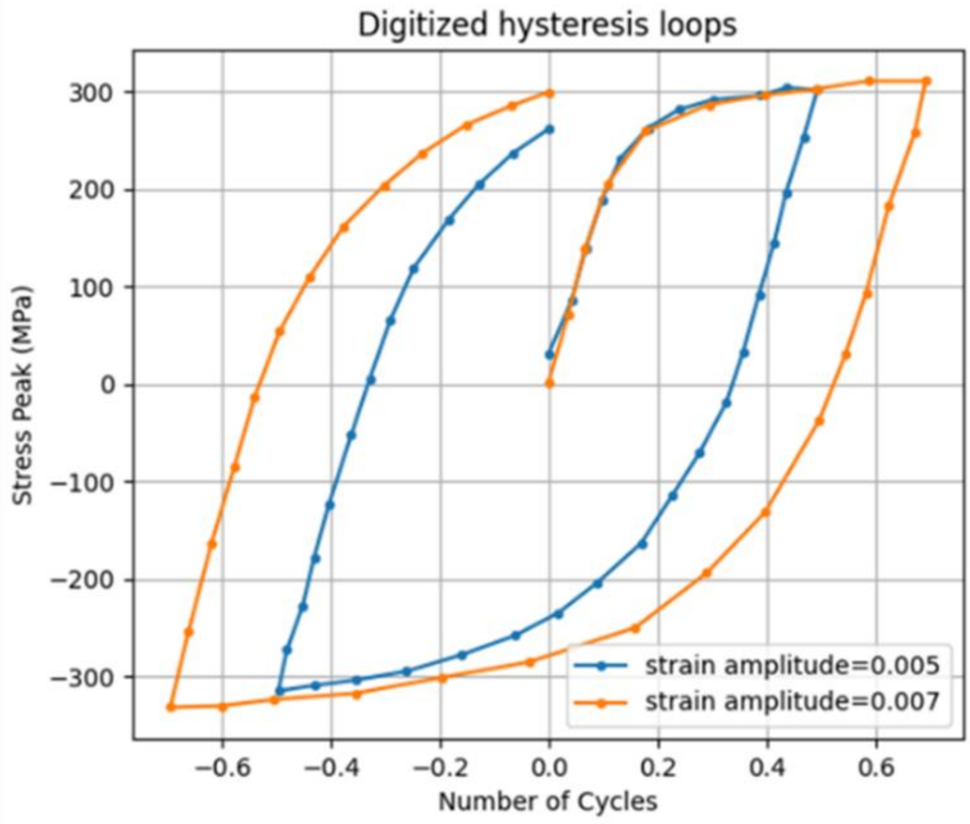

Figure 6 The first stress-strain hysteresis loop for 0.5% and 0.7% strain amplitude(Pelegatti et al., 2021; *WebPlotDigitizer*, n.d.)

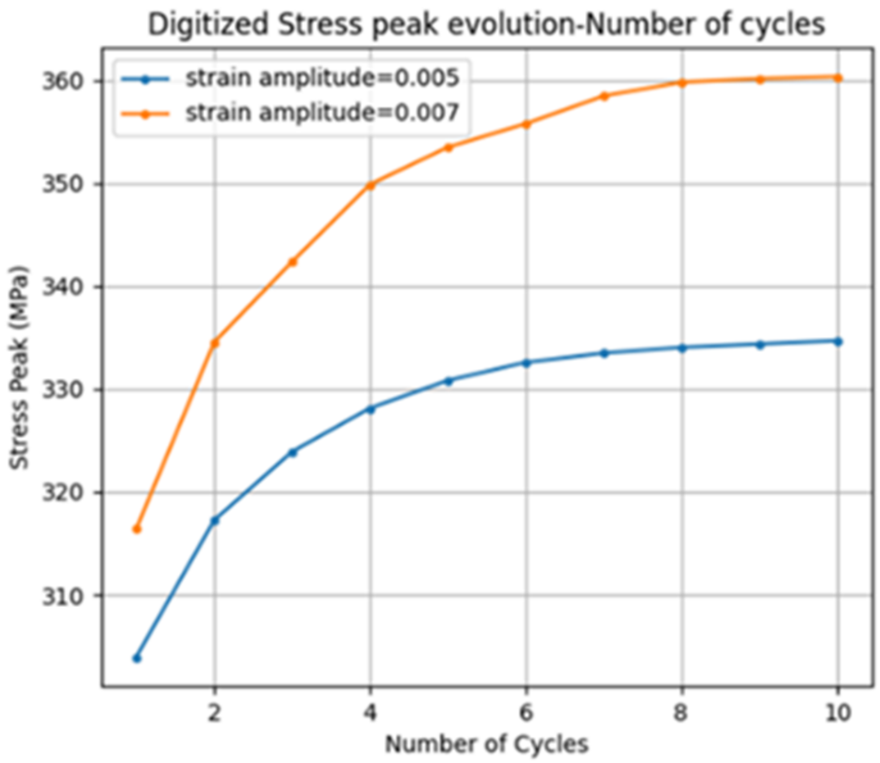

Figure 7 peak stress evolution for strain amplitudes of 0.5% and 0.7% (Pelegatti et al., 2021; *WebPlotDigitizer*, n.d.).

3.4.3 Interpolation and cyclic reconstruction

The experimental data available covers a limited number of cycles available (N = 1, 1000, 2000). To overcome this limitation, an interpolation method is used to estimate the intermediate stress-strain hysteresis loops via interpolation from the available experimental loops.

The interpolation procedure is used separately for each strain amplitude making sure that the strain amplitude-dependent hardening is captured from experimental evidence. Therefore, interpolation enables the creation of a continuous dataset that can be used in comparison with numerical simulations.

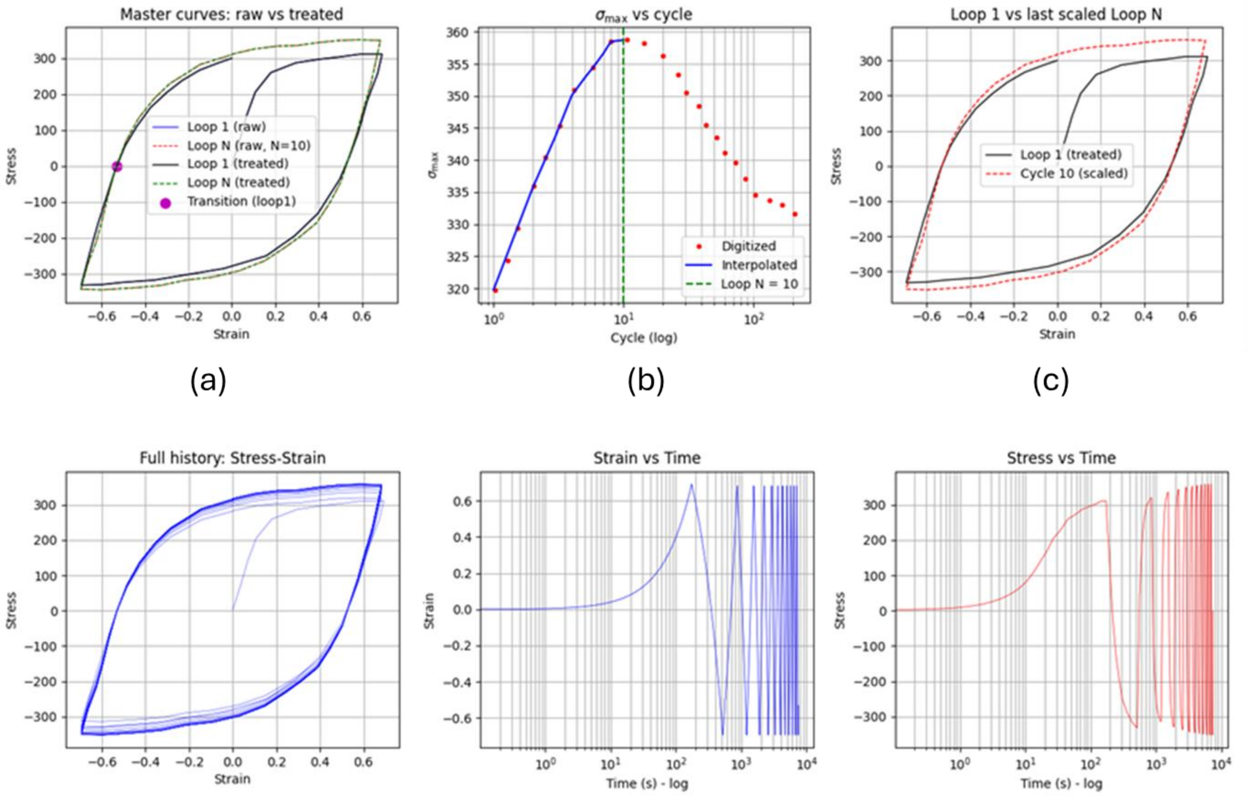

(a) (b) (c)

(d) (e) (f)

Figure 8 digitized and interpolated data for 10 cycles in strain amplitude of 0.007 (Pelegatti et al., 2021; *WebPlotDigitizer*, n.d.)

(a) Raw and treated digitized hysteresis loops used for cycle reconstruction

(b) Interpolated evolution of peak stress with cycle number

(c) Comparison between the first loop and the scaled stabilized loop

(d) Reconstructed full cycle stress-strain history

(e) Reconstructed strain history for cyclic loading

(f) Reconstructed stress response

3.4.4 Preparation of strain history input

The resulting strain histories are used as loading for simulation and the resulting stresses are compared to the simulated ones during optimization.

3.4.5 Extraction of Comparison Quantities

Key elements were extracted from both experimental and numerical results for the purpose of model validation and calibration. The main measurement for comparison is the maximum stress within a cycle, which is mathematically expressed as:
$S_{max}(N) = max(\sigma(t))$ within each cycle.
This parameter is determined individually for each level of strain amplitude. Besides that, the complete stress–strain curve is utilized to evaluate the fit of the stress-strain hysteresis loops.

3.5 Calibration Procedure

3.5.1 Simulation Setup

The experimental strain histories were reconstructed from the literature data using the approach presented in Section 3.4.3. These histories were then applied as loading input in the simulations of the cyclic tension-compression response of AISI 316L. In this way, the numerical experiments were kept fully consistent with the experimental setups.

3.5.2 1D projection of the model

For every possible set of parameters, an implicit integration method is used to solve the constitutive model subjected to strain-controlled loading. Then the calculated stress results are matched with the experimental results for both strain amplitudes. The series of parameter adjustments is stopped once changes of the objective function be-come smaller than the allowed tolerance. Using this optimization-driven scheme, it is guaranteed that the discovered parameters best represent both the cyclic hysteresis loops and the stress development during cycles. The following state vector at each strain increment is solved by one-dimensional implementation.

```
x = [s, e_pl, X1, X2, R1, R2, xi1, xi2, q1, q2]
x_new = fsolve(residuals, x0)
s[i]= x_new[0]
e_pl[i]= x_new[1]
X [i,:]= x_new[2:2+kinematic_cols]
R[i,:]=x_new[2+kinematic_cols:2+kine-
matic_cols+istropic_cols]
xi[i,:]=x_new[2+kinematic_cols+isotropic_cols:2+kine-
matic_cols+2*isotropic_cols]
q[i,:]=x_new[2+kinematic_cols+2*isotropic_cols:2+kine-
matic_cols+3*isotropic_cols]
```

3.5.3 Objective Function

A numerical optimization-based calibration procedure is used for identifying the material parameters by minimizing the deviation from the model response to the experimental data processed. Data of cyclic plasticity tests with two different strain amplitudes (0.005 and 0.007) are used for calibration.

The calibration is formally defined as a minimization problem of the following objective function:

$$\Phi(X) = \alpha\Phi_{hys}(\bar{p}) + (1-\alpha)\Phi_S \max(\bar{p}) \tag{17}$$

where $\bar{p}$ is the vector of material parameters. The main component Φ_{hys} corresponds to the error between the predicted and the experimental stress-strain hysteresis loops:

$$\Phi_{hys} = (1/N)\Sigma\left[\left(\sigma_{num} - \sigma_{exp}\right)/\sigma_{ref}\right]^2 \tag{18}$$

where σ_{num} and σ_{exp} are the calculated and measured stress outputs, respectively, and σ_{ref} is a scale factor equal to the maximum absolute value of the experimental stress. The auxiliary component $\Phi_S\max$ corresponds to the error in the simulation of the cycle-to-cycle change of the maximum stress.

$$\Phi_S max = (1/M)\Sigma\left[(S_{max}num - S_{max}exp)/S_{ref}\right]^2 \tag{19}$$

The definition of S_{max} is the peak stress during the cycle:

$S_{max}(\mathrm{N}) = \max(\sigma(\mathrm{t}))$

The scale factor S_{ref} corresponds to the maximum experiment value of S_{max}. To account for the relative importance of both the hysteresis loops and the cyclic stress evolution, a weight factor α= 0.5 is adopted.

3.5.4 Physical Constraints

To obtain parameter values consistent with reality, the following constraints are set during the optimization:

- The parameters for kinematic hardening must be positive definite $(C\_i > 0, D\_i > 0)$ The recovery rates should be ordered $(D\_2 > D\_1)$
- The memory parameters must be positive $(\mu\_i \geq 0)$
- The isotropic hardening parameters should be positive (Q_0, $Q\_sat > 0$)
- $Q\_sat > Q_0$
- Consistency between initial and saturation values of Q_0 and Q_sat.

3.5.5 Optimization Strategy

To guarantee global exploration and local refinement of the parameter space, a hybrid optimization strategy is adopted. First, a global search is done with the Differential Evolution global optimization algorithm. The result of the global stage is then taken as the starting point for a local gradient-based optimization using the (SLSQP) algorithm. Such a two-step method increases the calibration robustness and minimizes the likelihood of a local minima convergence. The constitutive model is characterized by parameters that need to be determined by calibration. These parameters and their meanings are given in Table 2.

Table 2 description of the model parameters

Constitutive Model	Parameter	Description
Armstrong-Fredrick Kinematic hardening	Ci	Hardening modulus
	Di	Dynamic recovery parameter
Isotropic hardening	Q0	Initial isotropic hardening value
	Q_sat	Saturation value of isotropic hardening
	b	Rate of saturation
Norton viscoplasticity rule	n	Exponent controlling rate sensitivity
	k	Viscosity parameter
Strain amplitude dependent hardening	mu	Memory evolution parameter

4 Results

4.1 Verification of the 1D Implementation Against Z-set Reference

Before employing the one-dimensional model to calibrate parameters, the numerical method was checked with the reference implementation in the Z-set material library. To guarantee a correct comparison, identical material parameters, loading cases, and time steps were applied in the two simulations. Figure 9 shows a comparison between the Python model and the Z-set standard model regarding strain amplitude, stress variation, stress-strain hysteresis loops, and total plastic strain.

4.1.1 Comparison of Results

The parameters for performing comparison are:

- Stress versus time (S11-Time)
- Stress versus strain loops (S11-E11)
- Strain versus time (E11-Time)
- Plastic strain evolution

Following the example, triangular waveforms with fixed strain rate are employed and at the same time step discretization is used in both cases.

The model response is obtained from:

- Python implementation developed in this study
- Standard Z-set model

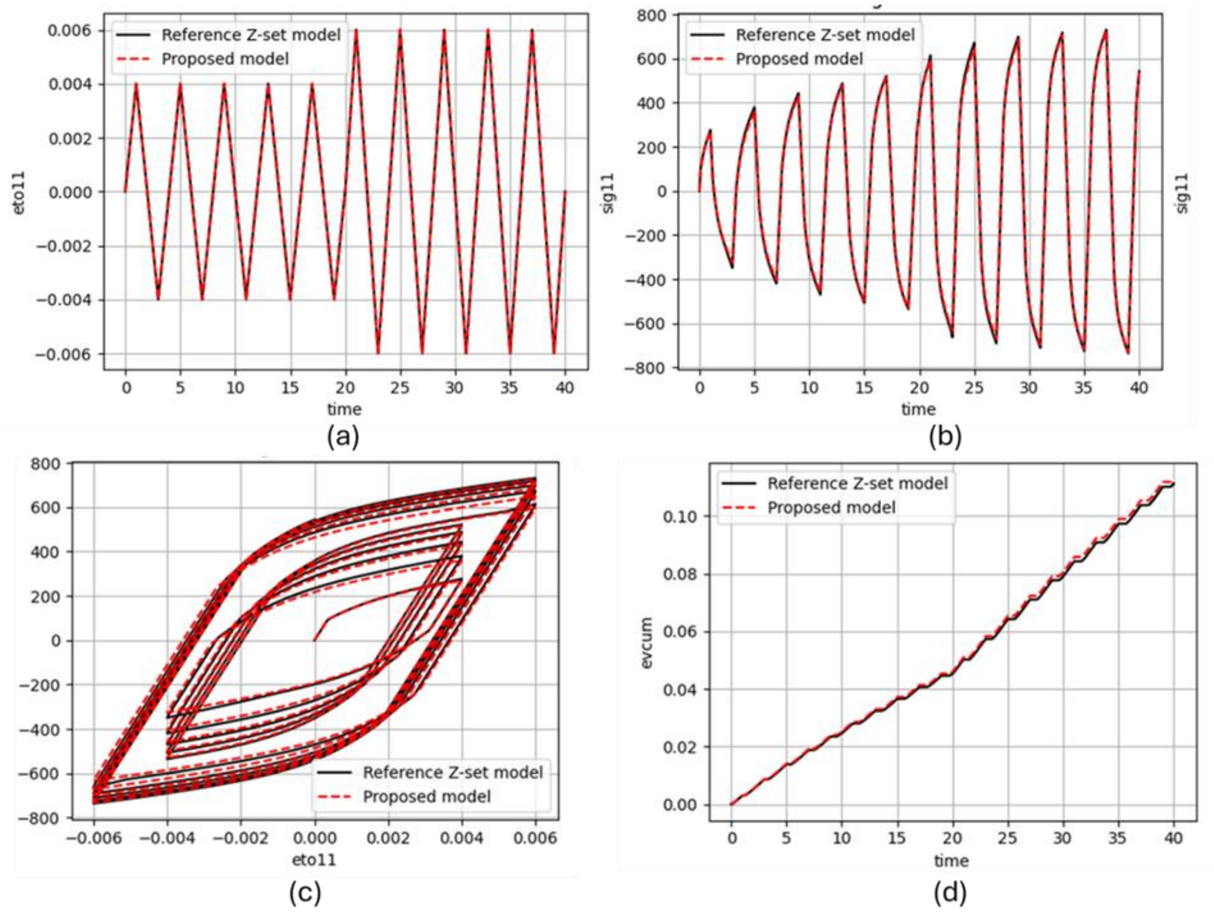

Figure 9 Agreement in comparison of the adopted model (strain amplitude dependent hardening with two isotropic) with the example in Z-set (Z-Set Material Model Manual: Memory Behavior, n.d.)

(a) **Strain-time diagram**

(b) **Stress-time diagram**

(c) **Stress-strain diagram**

(d) **Accumulated plastic strain diagram**

As shown in Figure 9, the result of the implemented model matches the reference Z-set solution for all quantities of comparison.

The correspondence of the stress–strain hysteresis loops confirms that the response to cyclic loading and unloading has been modelled correctly. The similarity in accumulated plastic strain is another evidence that the viscoplastic flow rule and the strain-amplitude-dependent hardening variables have been implemented in a consistent manner.

Consequently, the one-dimensional implementation is considered appropriate for the next calibration and validation stages.

4.2 Initial Model Prediction Before Calibration

Once the numerical implementation was verified; the response of the model was evaluated first without parameter calibration. This comparison was made to set a baseline response and to see the extent of the difference between the initial parameter set and the experimental cyclic behaviour of AISI 316L. Figure 10 shows the comparison of the initial model prediction with the experimental data in terms of maximum stress evolution and stress–strain hysteresis loops.

The stress-strain hysteresis loops predicted by the model have already captured the main features of non-linear cyclic behavior, including the transition between the loading and unloading phases. Besides that, the model has been able to reproduce stress evolution during the cyclic loading that is seen in experimental data.

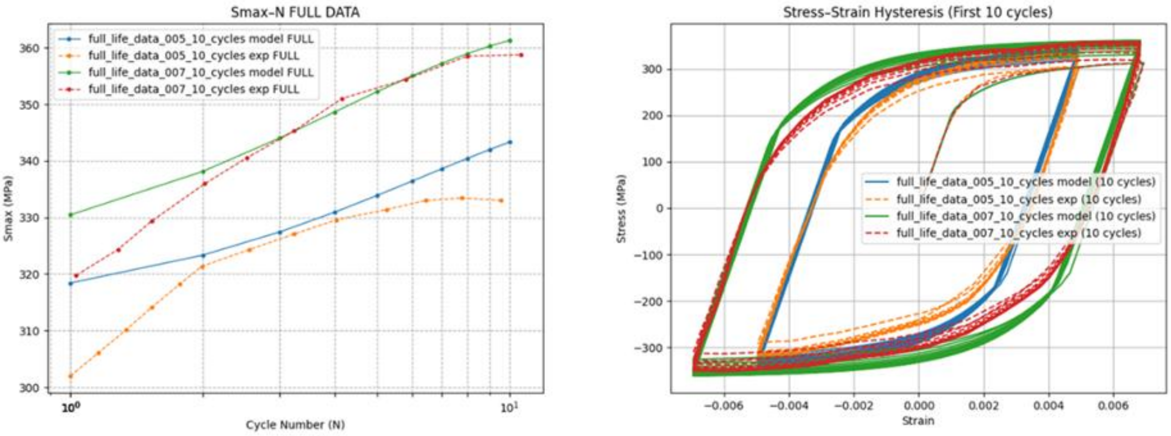

Figure 10 Initial model simulation for S-max-Number of cycles and hysteresis loops

Figure 11 demonstrates that the uncalibrated model is able to replicate the basic outline of the cyclic hysteresis phenomenon, however it cannot produce a sufficiently accurate quantitative match with the experimental data. Also, the differences are clear in the evolution of maximum stress and the size and height of the hysteresis loops. These inconsistencies reveal that the starting parameter set will not be capable of straightforwardly forecasting the cyclic response of AISI 316L. Therefore, the parameters need to be calibrated in order to get better matching between the numerical model and experimental results.

4.3 Parametric Analysis

A parametric study was carried out to gain insights into the physical role of constitutive parameters controlling cyclic plasticity evolution. The study concentrated on isotropic hardening parameters Q_0, Q_{sat}, μ, as these parameters have a significant impact on cyclic stabilization, stress evolution, and strain-amplitude dependent behavior.

4.3.1 Effect of Q0 on Cyclic Stress Evolution

The parameter Q_0 is controls the initial isotropic hardening part. Three different sets of Q_0 are selected to investigate the effect of this parameter while leaving all other calibrated parameters unchanged.

Table 3 Different values for analyzing the effect of Q0

Case	Q_{01}	Q_{02}
No Q_0	0	0
Calibrated amount	1.47	27.79
High Q_0	15	60

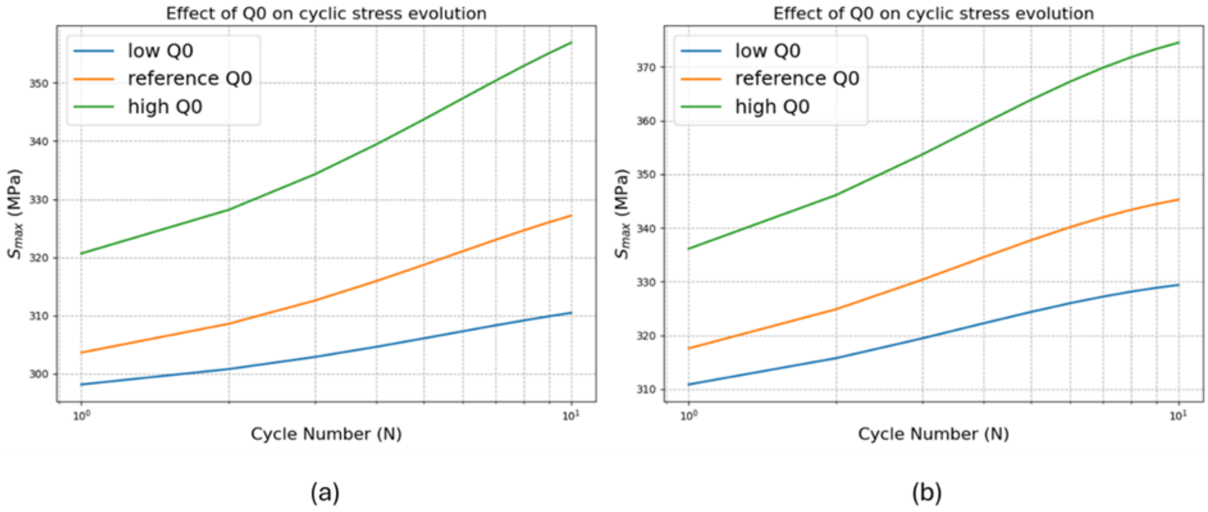

Figure 11 The effect of Q0 with different values for strain amplitudes of (a) 0.005 and (b) 0.007

Results indicate that changing Q_0mainly affects the early cyclic response and the first loading cycles. In both figures, the lowest amount of Q_0 is 0 which means that there is no initial isotropic hardening, and the difference between the saturated stress level and the first cycle stress would be very low. Larger values of Q_0raise the initial stress level and postpone the turning point to stabilized behavior and lowering Q_0 reduces the initial isotropic hardening component. It is also illustrated that the higher strain amplitude is more sensitive to changing the value of Q_0.

4.3.2 The Effect of Q_{sat}

The Q_{sat}parameter controls the long-term isotropic hardening behavior and stress levels that have reached the stabilized stress level.

Table 4 Different values for analyzing the effect of Q_{sat}

Case	Q_{sat1}	Q_{sat2}
Low Q_{sat}	7	20
Calibrated Q_{sat}	27.064242	60.984990
High Q_{sat}	100	150

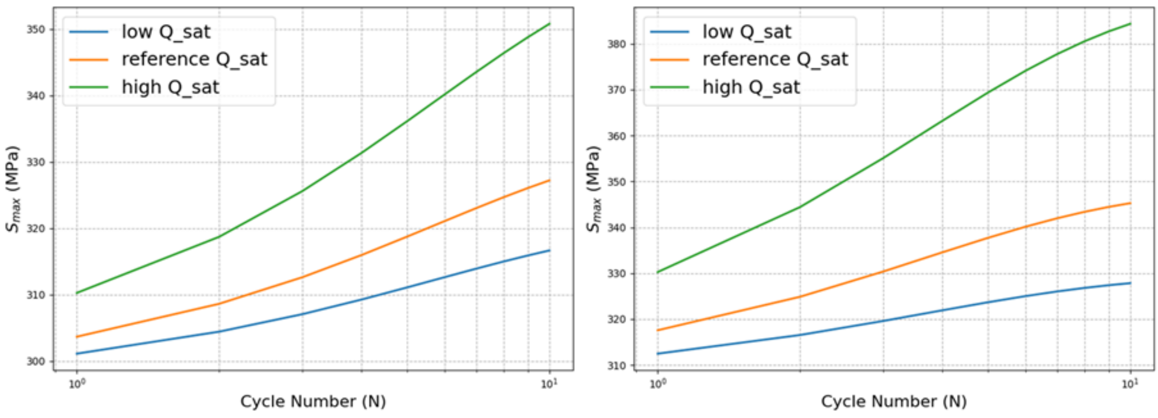

(a)

(b)

Figure 12 Influence of the Q_{sat} parameter on the Smax–N response for strain amplitudes of (a) 0.005, and (b) 0.007.

Increasing the Q_{sat} parameter will increase the stabilized cyclic stress levels as well as making stress saturation happen later. On the contrary, low values result in faster stabilization and smaller stress amplitudes under cyclic loading conditions. According to the results, Q_{sat} controls the long-term cyclic hardening rather than the initial isotropic hardening. It is also concluded that the higher stress amplitude is more sensitive to changing this value.

4.3.3 The Effect of μ in strain amplitude dependent hardening

The parameter μ controls the strain-amplitude dependent hardening effect in the constitutive model.

Table 5 Different values for analysing the effect of mu

Case	μ_1	μ_2
Low μ	0.1	5
Calibrated μ	5.85	52.40
High μ	100	500

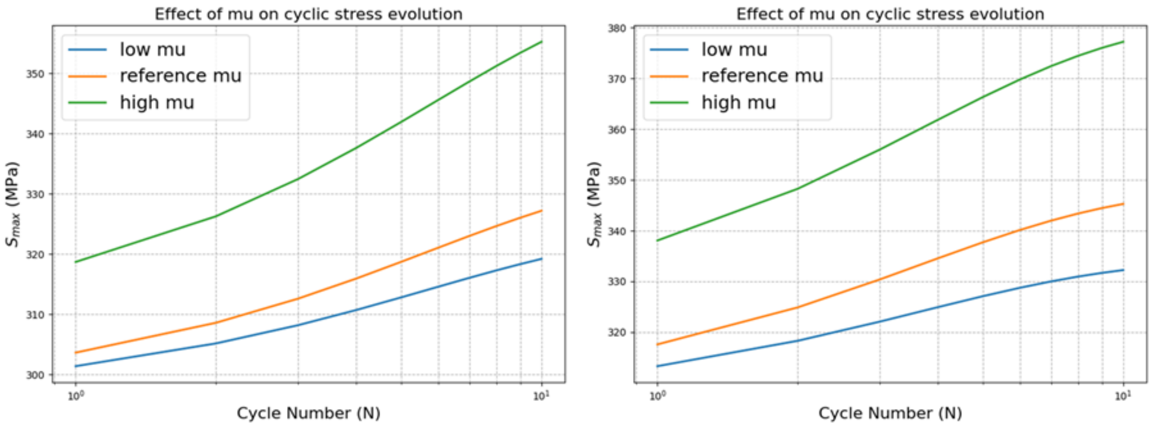

(a) (b)

Figure 13 Influence of the parameter μ on the Smax–N response for strain amplitudes of (a) 0.005, and (b) 0.007

The results indicate that increasing μ enhances the strain-amplitude sensitivity of the constitutive response. As a result, the stress evolution becomes more dependent on the previous loading history and accumulated cyclic deformation. This behavior is particularly important for reproducing the different mechanical histories observed at pipe hotspots subjected to different strain amplitudes. The more μ increases, the more separation between cyclic stress evolution would be seen for different strain amplitudes. This behavior shows that this constitutive model can reproduce different mechanical histories based on the cyclic loading conditions implemented. It is also clear that at higher strain amplitudes, increasing μ has higher effect on raising the stress level.

4.4 Calibration Results

4.4.1 Calibration over 10 Cycles

After optimizing for 10 cycles, the model shows a significant improvement in reproducing the experimental response. Subsequently, the stress–strain hysteresis loops closely match the experimental curves in terms of loop width, peak stress, and cyclic evolution. The nonlinearity of the loading and unloading branches is well captured, which means that the kinematic hardening formulation accurately represents the model response.
The progression of S-max is also well reproduced. The model captures the rapid in-crease in stress during the initial cycles, and there is good agreement from the first cycle.

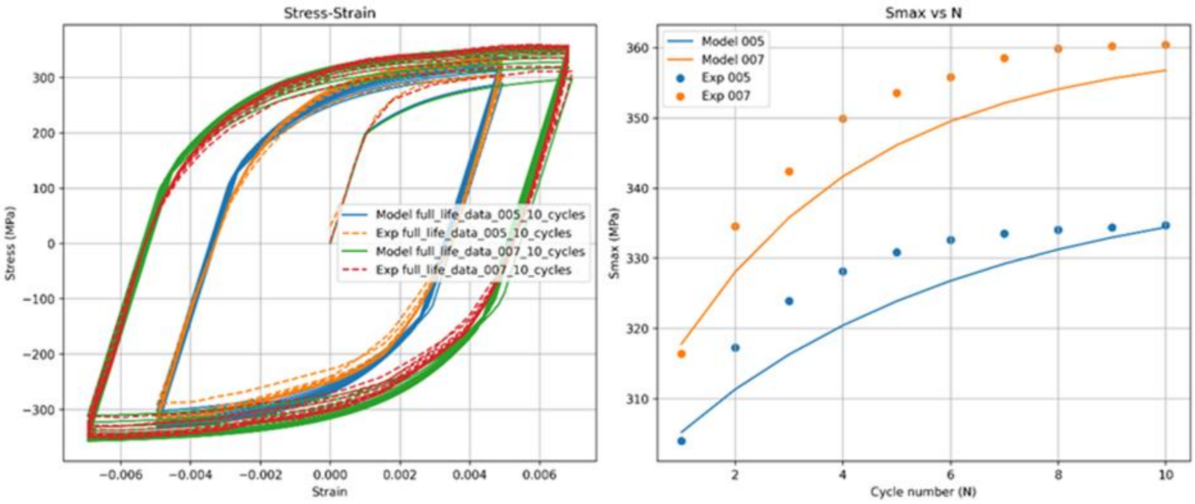

Figure 14 Hysteresis loops and Smax-N calibration for 10 cycles

As mentioned in section 3.5, the model is supposed to capture a representative stabilized cyclic response which offers a physically meaningful average stress state for the following structural and fatigue-related analysis.
The enhanced constitutive model was validated by comparing its numerical results with the experimental cyclic responses measured at different strain amplitudes. This part aims at testing the ability of the proposed formulation to reproduce cyclic plasticity, stress evolution, and stabilization features experimentally observed.

4.4.2 Generating stabilized behavior of calibrated strain amplitudes (0.005, 0.007)

To begin with, the cyclic responses from experiments at the strain levels of 0.005 and 0.007 are used to illustrate the cyclic hardening and saturation behavior of the material. These loading cases were basically used during the calibration step of the constitutive model. In the next section, the results from the calibrated model are compared with experimental hysteresis loops and stress evolution plots for different strain amplitudes. The model does not have softening and is representative of the maximum stress that is obtained experimentally. After the maximum level of the stress the model flats down without softening because the maximum stress here is the conservative measure of the stress range. According to figure 15, the first point in the model and the ending point of 10 cycles match well with the experimental values. While other points are not aligned well, the starting and ending points are important because the first point can control how well the assembly loads could be described.

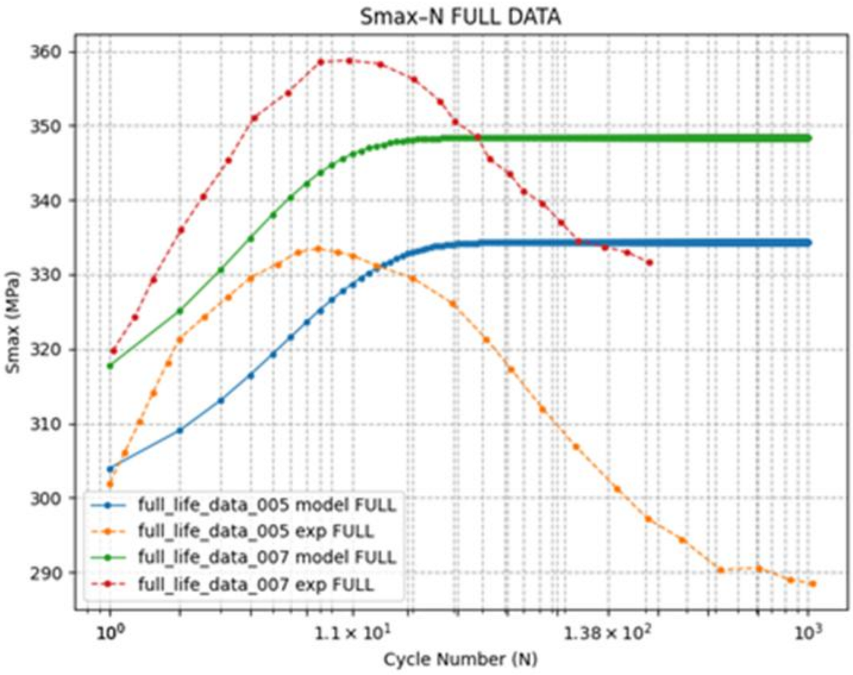

Figure 15 Simulation of proposed model with calibrated parameters for strain amplitudes of 0.005 and 0.007

4.4.3 Parameter Calibrated results

In order to quantitatively evaluate how well the model performed, the relative error of the maximum stress predicted was evaluated. For the two strain amplitudes considered, the relative error remained in an acceptable range, showing that the numerical prediction and experimental data matched well. This confirms that the method of finding parameters produced an appropriate set of parameters capable of reproducing stabilized cyclic behavior. The final material model parameters are given in table 6.

Table 6 Calibrated parameters of the material model

Parameter	Calibrated value
n	6.887065
k	42.375060
D1	329.945927
D2	993.192779
C1	21586.239288
C2	42092.141907
M1	0
M2	0
m1	1
m2	1
Qsat1	27.064242
Qsat2	60.984990
Q01	1.472346
Q02	27.788221
mu1	5.857819
mu2	52.406089
b1	1014.666581
b2	12.998533
R0	190

4.5 validation of the resulting model with unseen data

After the parameter set was calibrated, the model's robustness evaluation was performed by using it for additional strain amplitudes that were not included in the calibration data. The predicted responses of maximum stress versus number of cycles (Smax-N) show physically meaningful trends for all cases studied. The higher strain amplitudes show higher stabilized stress level and cause the material to harden faster initially. The model shows consistent qualitative behavior and illustrates that it is able to generalize beyond the calibration conditions.

The first 10 cycle data is gathered for different strain amplitudes from the literature (Pelegatti). The model is tested against experimental data in the simulation, and a good agreement could be seen from figures 16 and 17. The experimental data is shown by dash lines, and the model is indicated with solid lines.

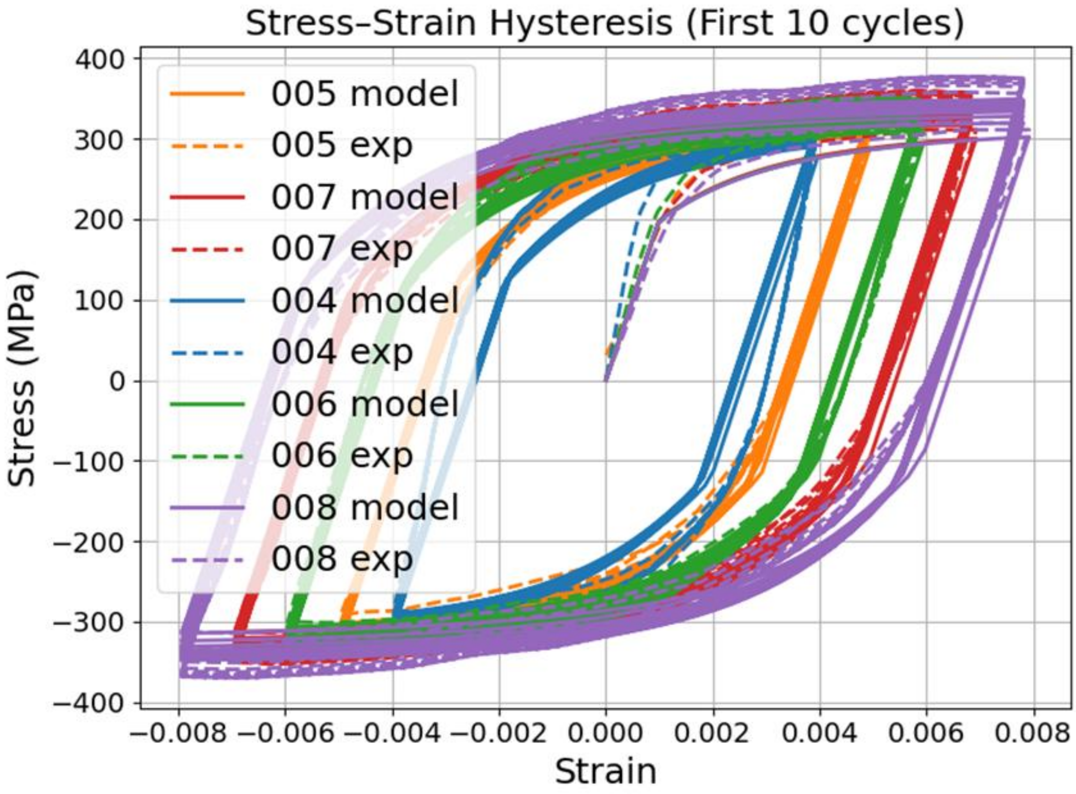

Figure 16 Behavior prediction of constitutive model (stress-strain) against experimental data for different strain amplitudes for 10 cycles.

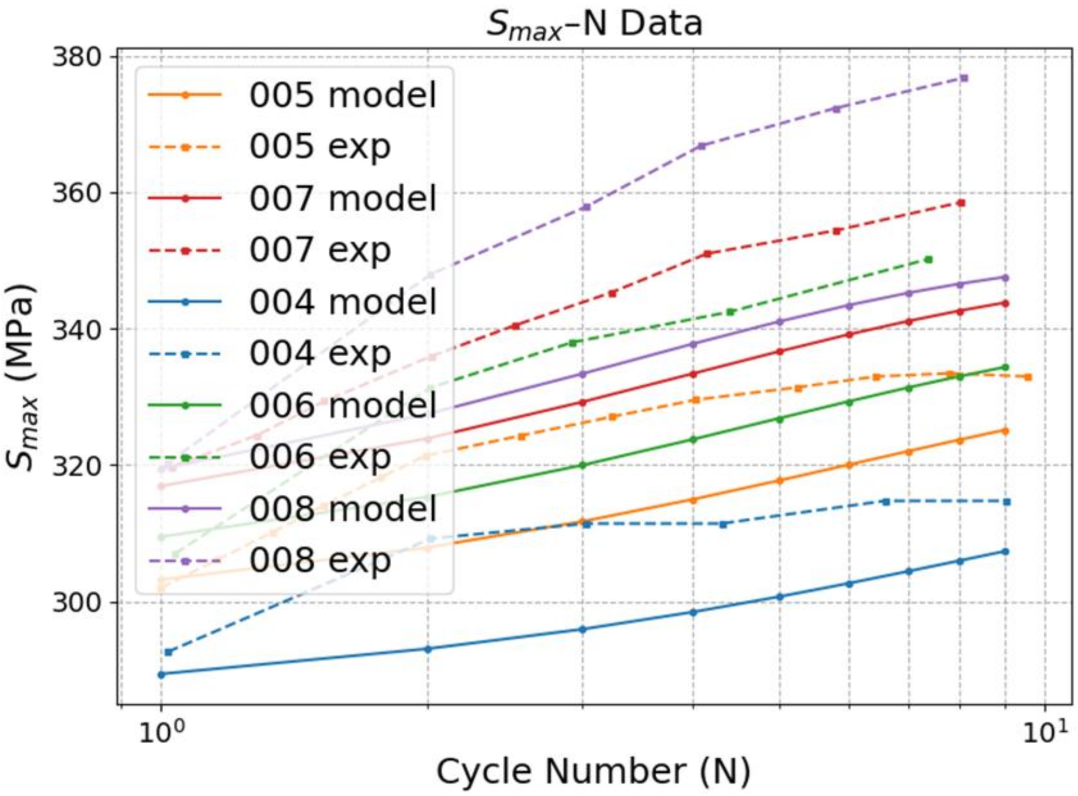

Figure 17 Behavior prediction of constitutive model (stress-strain) against experimental data for different strain amplitudes for 10 cycles.

The model then predicted 1000 cycles for all the strain amplitudes that are unseen data mentioned above and the stabilized behavior could be seen after the first hardening for all strain ranges.

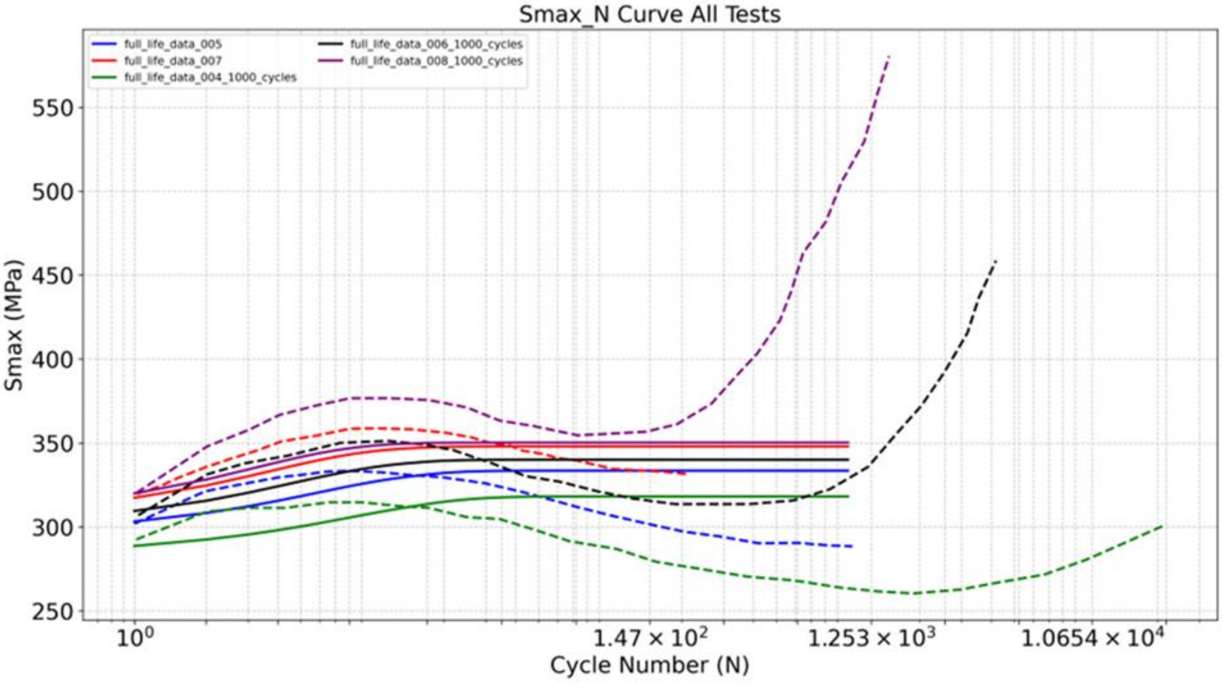

Figure 18 Evolution of Stress–Number of cycles for 1000 cycles in different strain amplitudes

4.5.1 Application of the Calibrated Constitutive Model in a Gas Manifold

4.5.1.1 ABAQUS global model analysis

The global analysis is done to evaluate the structural response of the installed gas-system under combined service loading. The loading conditions included gas pressure up to 10 bar[g], gas temperature variation from −20 to +80 °C, bolt pretension, thermal loads, nominal pressure loads, and assembly displacement according to the drawings. The analysis provided the overall distributions of stress, plastic strain, displacement, and flange contact behavior, which formed the basis for selecting the local region for further submodel analysis. The global finite element model represents the W18V46TS-DF/SG gas-system assembly in its surrounding engine environment. The model includes the main gas-system components, such as the gas inlet pipe, gas manifolds, supports, degassing valve, associated piping, inter-cylinder pipe, SOGAV assembly, and crankcase breather, together with relevant engine structures (figure 19a) needed to represent the overall stiffness and loading conditions of the assembly.

4.5.2 Abaqus Submodel Analysis

Once the constitutive model was calibrated, the material parameters determined were implemented in a finite element framework through ABAQUS to study how they could influence the predicted stress distribution estimated in a real engineering part.

To use less time, a submodel approach is used and the boundary conditions are implemented from the global model. The component analysed is a gas manifold system with local stress concentration in marine engines, which experiences cyclic loading conditions during operation. The initial global finite element model was based on an elastic–perfectly plastic material model of AISI 316L steel components. The implementation of cyclic plasticity model makes it possible to directly compare the differences between a simplified and physically enriched material models regarding their influence on the stress prediction.

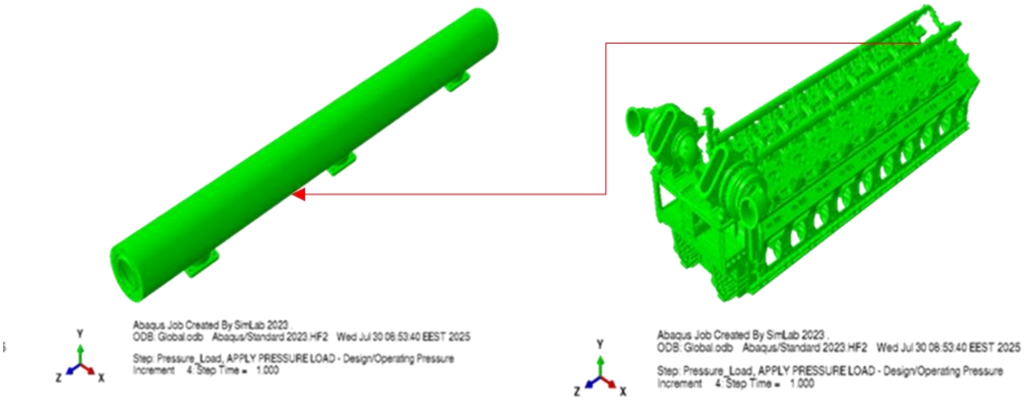

(a) (b)

Figure 19 (a)The representative pipe as the submodel and (b)the global model in ABAQUS

4.5.3 Submodel results

A submodeling strategy was adopted to enable detailed local analysis while maintaining computational efficiency. The submodel area that was chosen for this purpose corresponds to the critical zone of the gas manifold where the highest stress concentrations were found in the global model.

Submodel boundary conditions were derived from the displacement field of the global model. Nodal displacements obtained from the global model were implemented as boundary conditions on the submodel's cut surfaces.

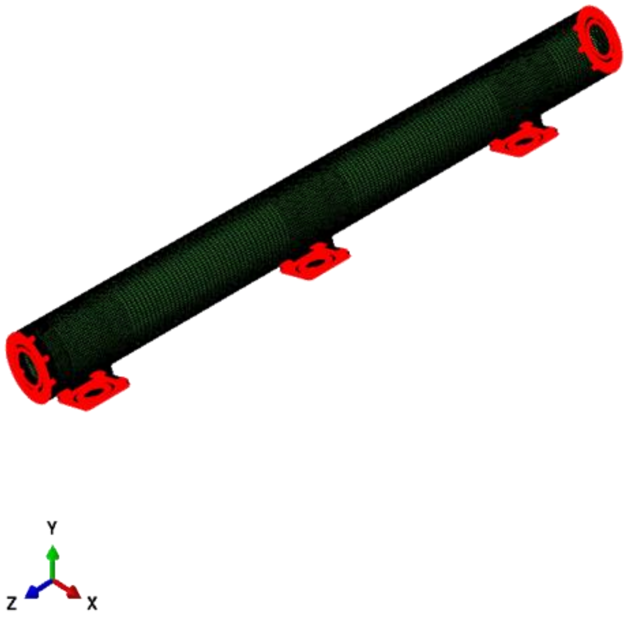

Figure 20 Connected surfaces of submodel to the global model for implementation of the boundary conditions

The load was also implemented according to the global model on the related surfaces according to the global model as shown in figure 21.

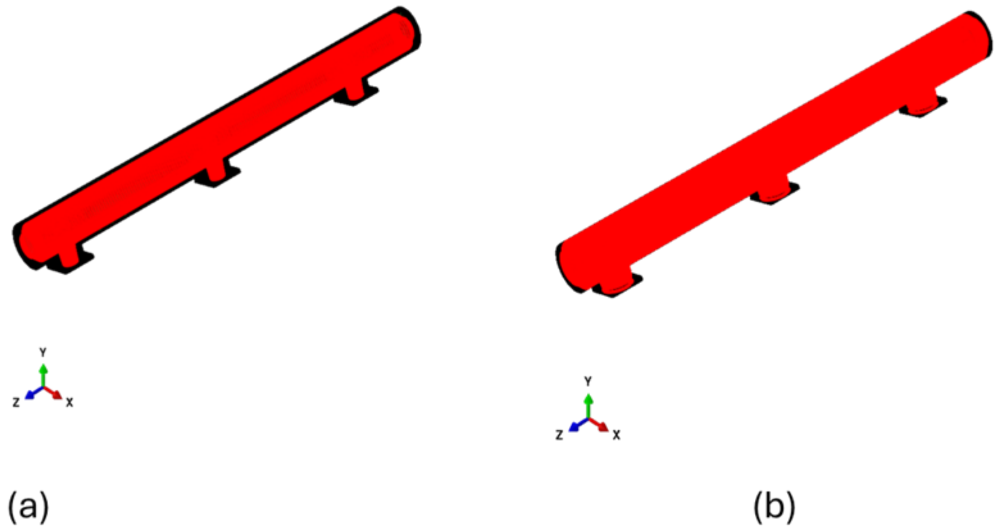

Figure 21 Inner and outer surfaces of the pipe for implementation of the load from the global model

This approach ensures that the submodel experiences the same global deformation state while allowing the local stress–strain response.

4.5.4 Submodel Validation Using the Basic Material Model

4.5.4.1 Contour comparison

Before introducing the advanced material model, the submodel was checked against the global model for consistency. Both the models were subjected to similar elastic–perfectly plastic material characterization.

The comparison shows good agreement between the two models in terms of the displacement and the stress fields. The displacement pattern at the submodel boundaries closely follows that of the global model, which proves that the boundary conditions have been properly transferred.

Similarly, the von Mises stress pattern in the submodel also agrees with the global solution.

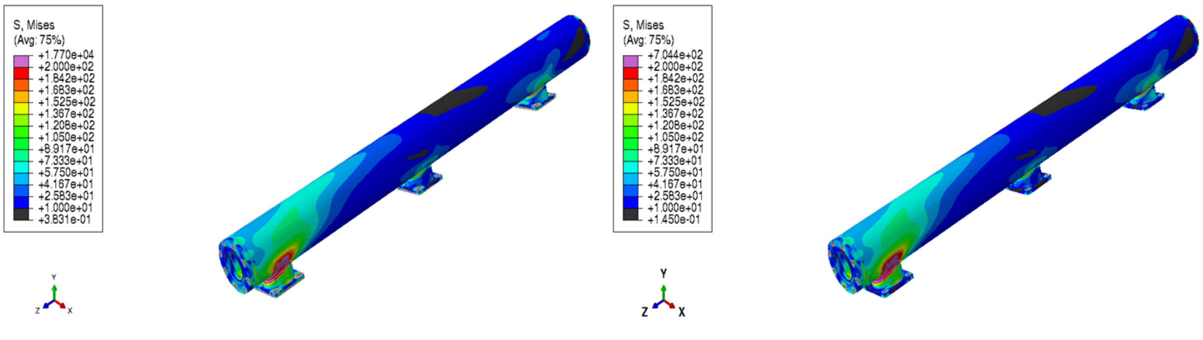

(a) (b)

Figure 22 stress contour match in (a) submodel and (b) global model

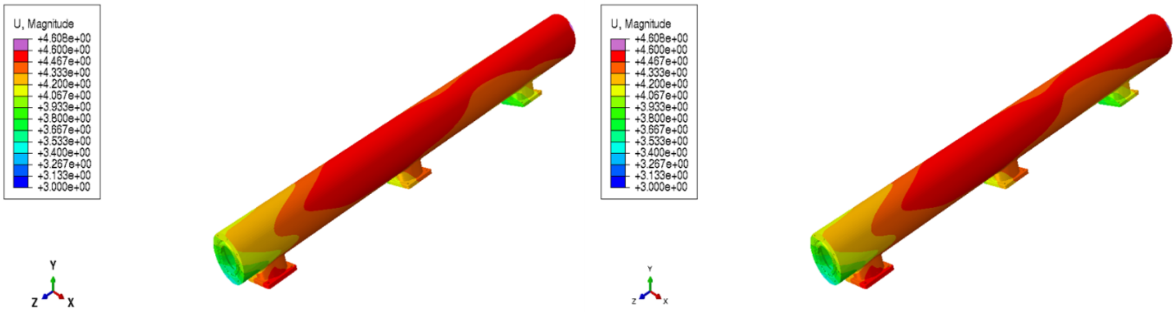

(a) (b)

Figure 23 Displacement contour matches in (a) submodel and (b) global model

4.5.4.2 Local Stress and Strain History Comparison

To check the accuracy of the submodel and ensure that it can act as the global model, the stress-strain and stress-time diagrams are plotted and checked for nodes with different locations. A Location with low stress is selected to show that in parts of the submodel far from the boundary conditions and in elastic regions, the stress histories should match well with the global model. In locations with high stress values, where the material enters plasticity, the submodel results will not match exactly with the global model

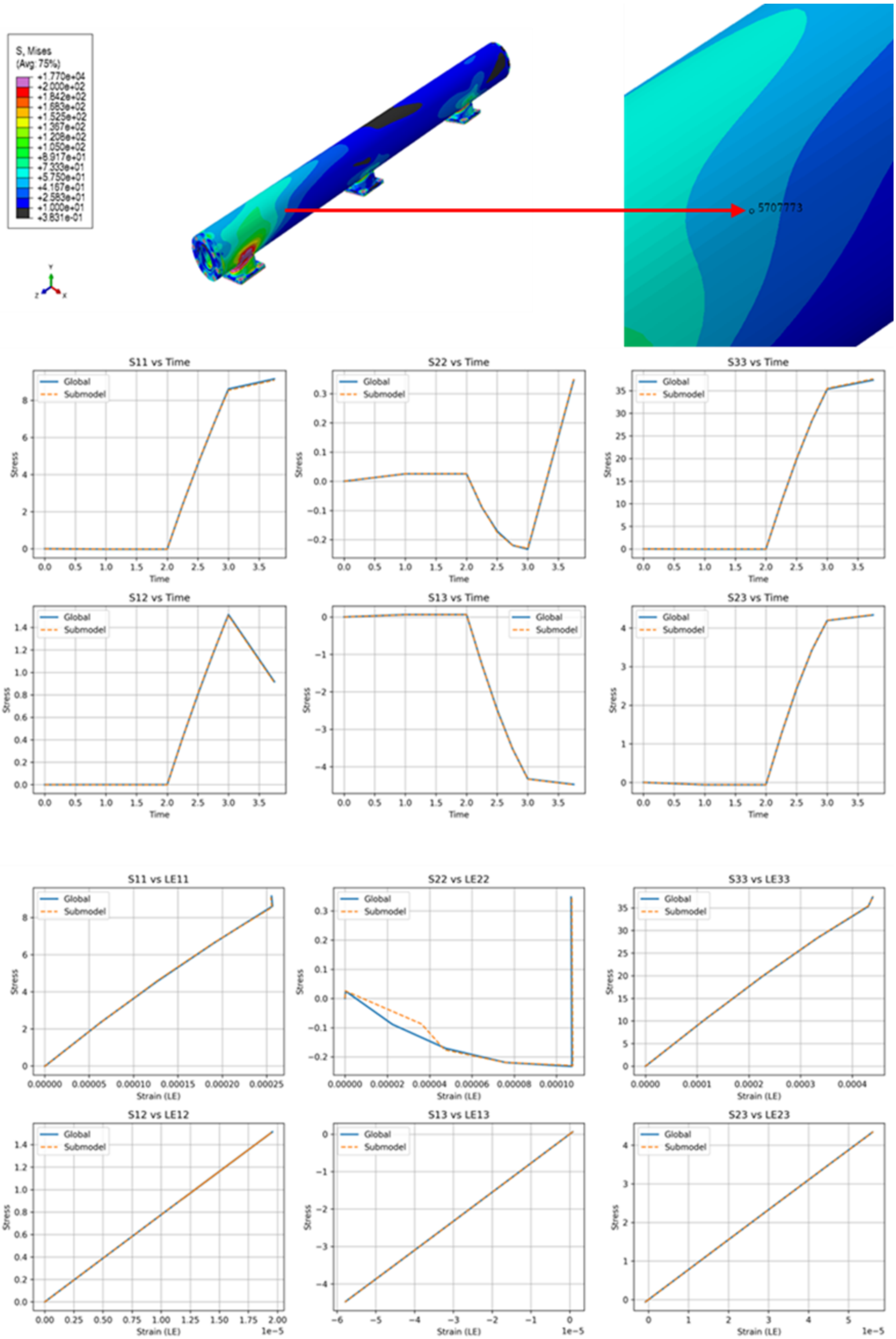

Figure 24 Selection of a node (5707773) with a low stress value and extracting the stress-time and stress-strain history in the basic model and submodel

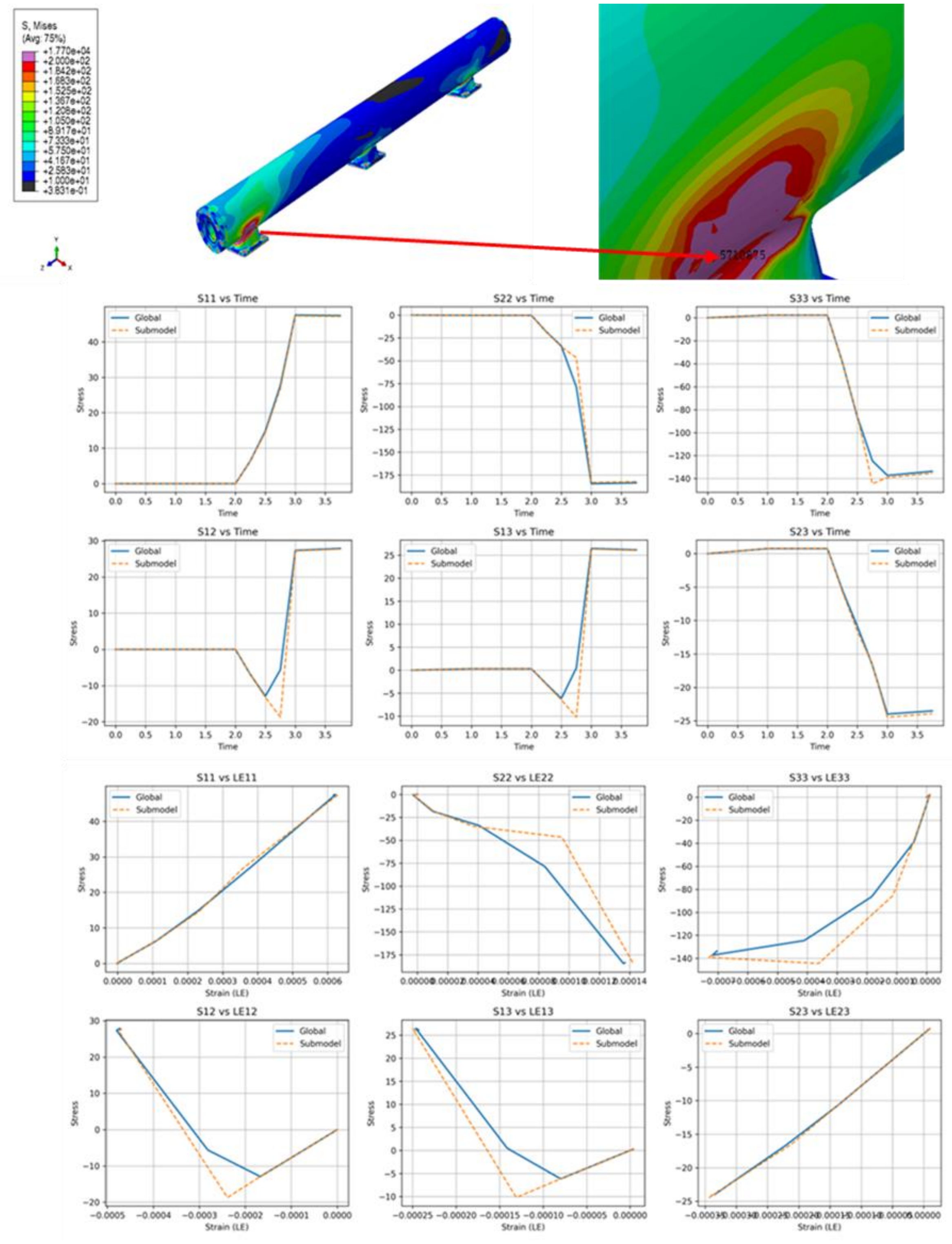

Figure 25 Selection of a node (5710928) with a high stress value and extracting the stress-time and stress-strain history in the basic model and submodel

4.5.4.3 Validation summary

The validation results show that the developed submodel reproduces the mechanical response of the reference global model accurately when identical material assumptions are considered. The contour comparisons and the local stress–strain histories both show close agreement between the two models, which confirms that the strategy of submodeling and boundary condition transfer are sufficiently representative for the current analysis. Therefore, the submodel is considered validated for further constitutive model assessment.

5 Discussion

5.1 Implementation of the enhanced Constitutive Model

Initially, the submodeling strategy was verified using the basic material formulation, and the constitutive model was then developed to incorporate a more advanced cyclic plasticity model.

The reference analysis was based on a simple elastic-plastic model without hardening, where the yield surface remains fixed after yielding, and no hardening evolution is considered after plastic deformation.

The improved constitutive model implemented in this study includes nonlinear kinematic hardening, isotropic hardening, viscoplasticity, and strain-range dependent behavior. The model was implemented through the Z-mat constitutive framework and coupled with the finite element simulation environment of Abaqus.

The incorporation of nonlinear kinematic hardening allows the constitutive model to represent the yield surface translation evolution during cyclic loading, whereas iso-tropic hardening controls the size evolution of the yield surface. Furthermore, Viscoplasticity introduces the rate dependency in the inelastic deformation behavior, and the strain-memory model permits the material to respond in a way that de-pends on the previously experienced deformation history.

The updated constitutive model, different from the base elastic-plastic model, lets the local mechanical behavior change gradually during the plastic deformation phase. Therefore, regions with different local strain levels are no longer forced toward a common saturated stress response after yielding. Instead, the constitutive response continues to be influenced by the local deformation history and hardening evolution.

The reason behind adopting the new constitutive model is, therefore, not just to change the level of stress, but also to better represent the local cyclic mechanical behavior in the most critical regions that are relevant to fatigue assessment.

5.2 Stress Redistribution and Contour Comparison

The comparison of the stress contours reveals an evident difference in the local stress redistribution behavior which is predicted by the two constitutive formulations. Although similar critical regions are identified in both models within the structure, the development of the local stress field differs significantly once plastic deformation develops. In the basic elastic–perfectly plastic model, the stress at the critical hotspot rapidly approaches a saturated level after yielding. Consequently, the surrounding regions progressively carry a larger portion of the applied load, leading to a relatively diffuse stress redistribution pattern around the hotspot region.

In contrast, the enhanced constitutive model predicts a more persistent localized stress concentration at the critical spot. Local material resistance keeps on evolving during plastic deformation through nonlinear kinematic hardening, isotropic hardening, viscoplasticity, and strain-history dependent changes. Therefore, the hotspot is expected to remain mechanically active during the entire loading sequence instead of rapidly transitioning toward a saturated stress state.

The regions of the postage stamp square contours comparison indicate that the enhanced constitutive model supports the existence of a very local stress distribution near the critical hotspot, whereas the basic model generates a more diffused distribution of stress around the material.

From an engineering point of view, the difference is particularly important since the behavior of local stress concentrations strongly influences the fatigue critical zones and the development of cyclic mechanical response in the gas manifold structure.

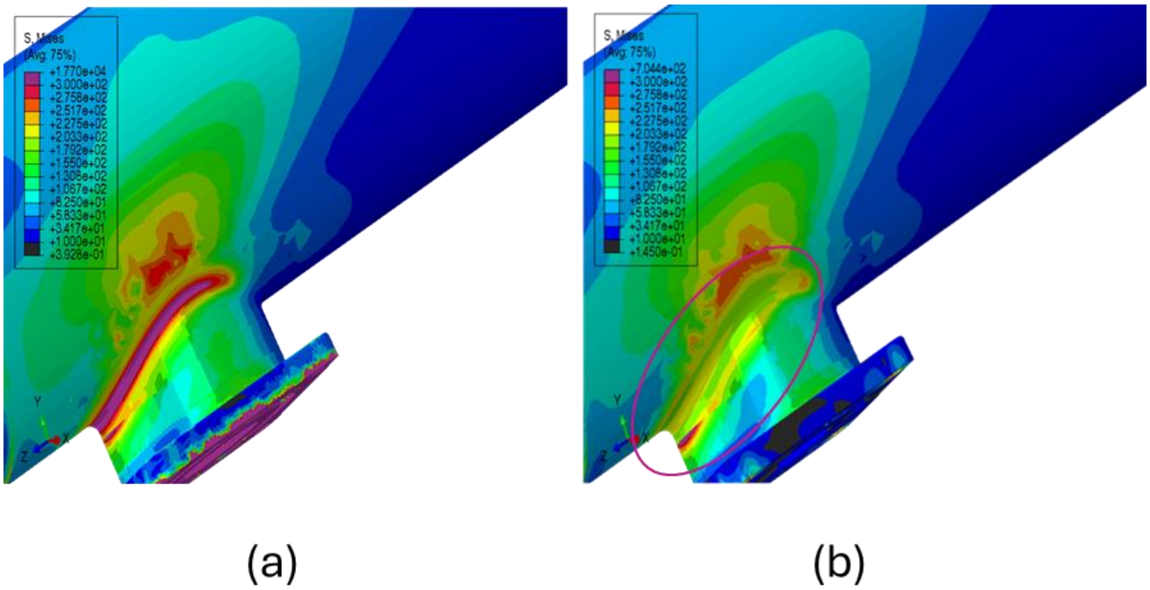

Figure 26 Comparison of local stress redistribution and stress concentration behavior be-tween (a) the enhanced material model (b) the basic elastic–perfectly plastic material

5.2.1 Constitutive evolution at comparable hotspot condition

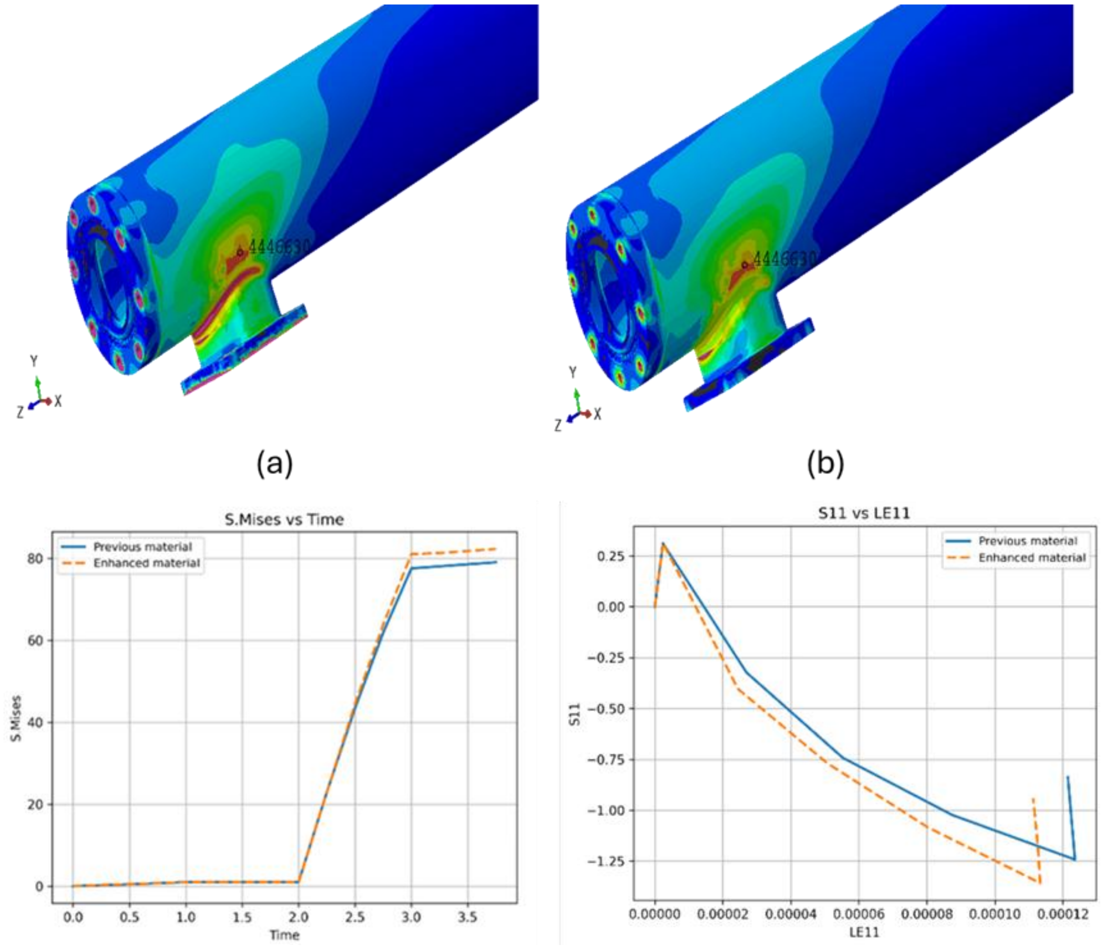

Figure 27 Representative low stress node in (a) model with enhanced material and (b) the base model and comparison of the stress–time and stress–strain response at this node (4446690) where the predicted stress remains below the material yield stress.

Initially a representative point was selected from a low-stress zone where the predicted stress levels did not exceed the material yield stress. The main purpose of this comparison is to check the consistency of the two constitutive formulations before significant plastic deformation.

The stress–time and stress–strain curves reveal that the two models produce almost identical local responses here. Since the local stress level does not reach the yield stress, the behavior of the structure is dominated primarily by elastic deformation. Therefore, the effect of constitutive hardening evolution remains limited.

In fact, this observation confirms that the variations noticed later in plastifying hotspot areas are mainly associated with the constitutive treatment of plastic deformation and not to the numerical differences between the models.

5.2.2 Local stress concentration in plastified locations

The main low-stress region showed a similar behavior in both constitutive formulations. However, once plastic deformation develops, more significant differences emerge. To assess the effect of constitutive hardening behavior in plastic conditions, two hotspots were selected from critical regions in the basic model where the local stress is higher than the material yield stress. These locations are the structurally critical regions which are supposed to govern the local cyclic mechanical response of the manifold.

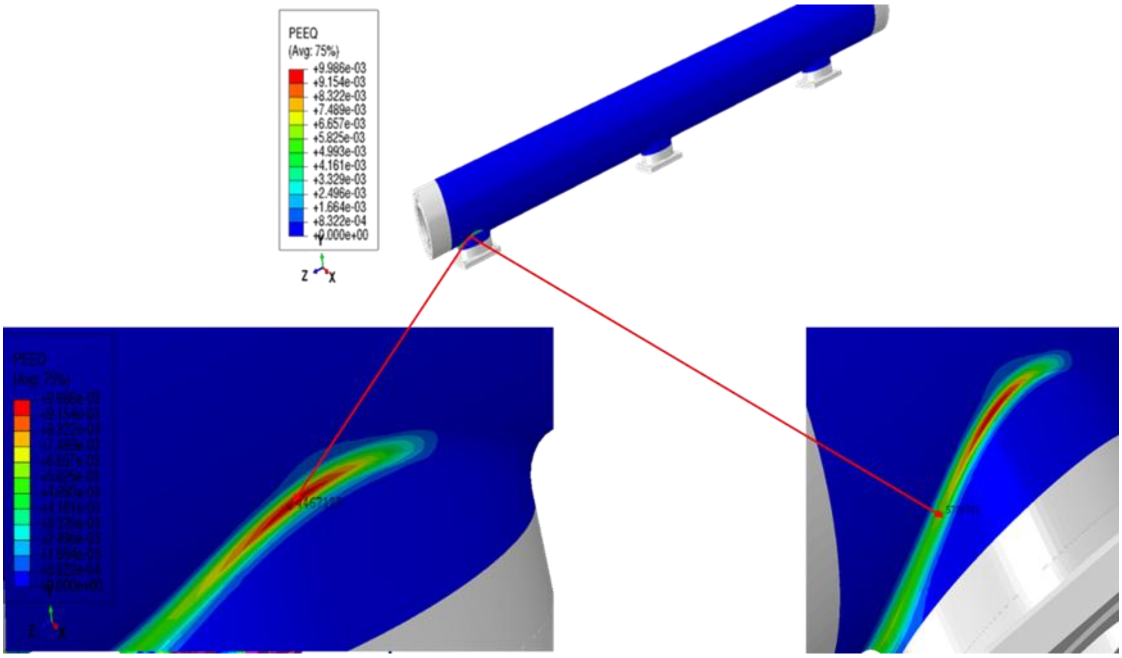

Figure 28 Location of the selected plastified hotspot regions in the global model used for local constitutive response comparison

The chosen hotspots are distributed in the plastified regions where the basic model shows high local stress concentration. While all the points are from mechanically critical regions, the local stress and strain histories are different. The reason for selecting these points is to check if the constitutive formulation captures the effect of local de-formation history on the predicted response of the hotspot.

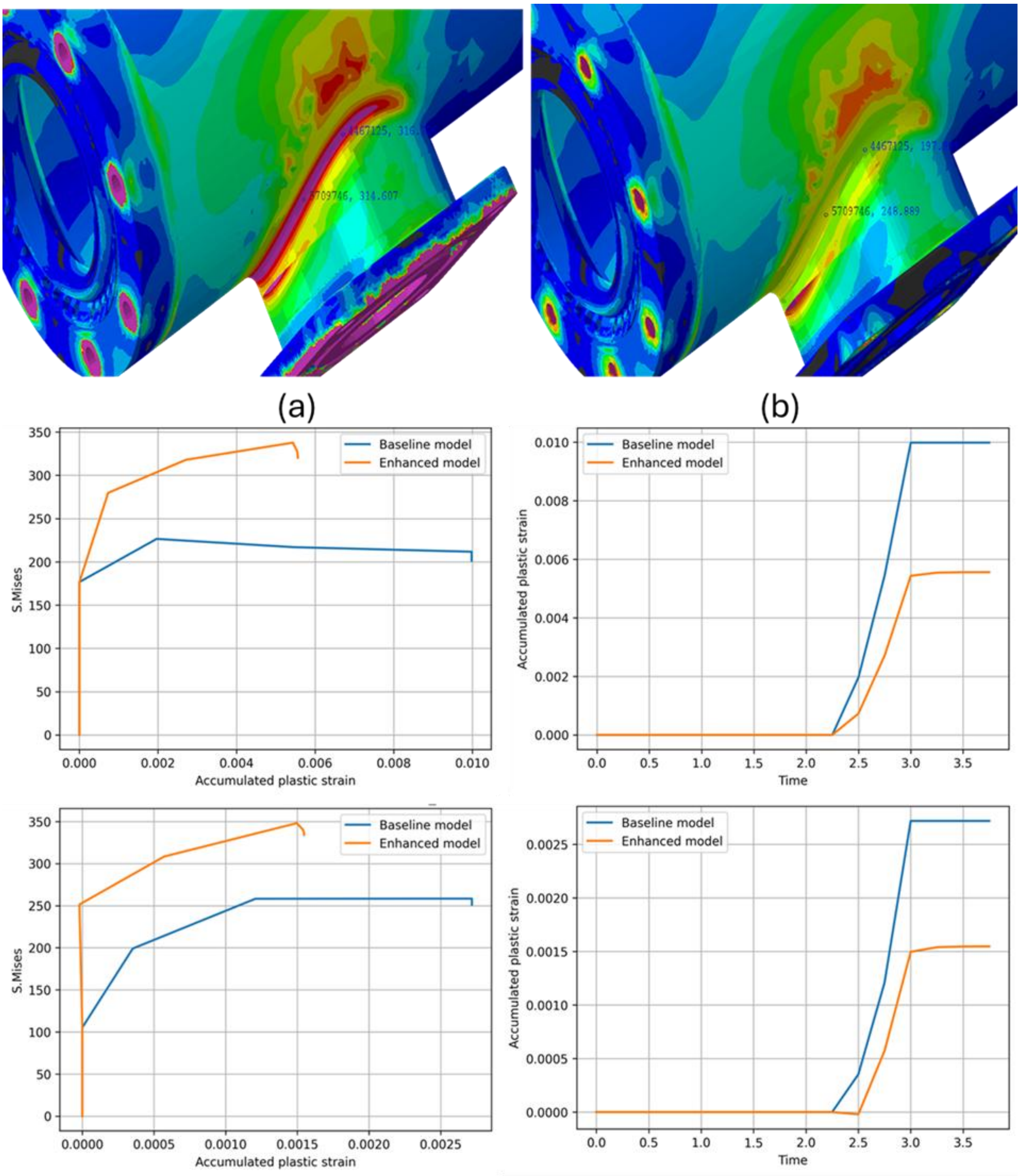

Figure 29 Comparison of von Mises stress distribution near the selected plastified hotspot regions (nodes 4467125, 5709746) for (a) the enhanced constitutive formulations and (b) the basis model with S. Mises-LE11 and S. Mises-Time diagrams.

The contour comparison near the chosen hotspot regions reveals that the constitutive model affects not only the local stress values but also the pattern of stress distribution around the plastified zones.

Even though both models point out similar critical spots, the advanced constitutive formulation shows a different local stress pattern compared to the basic elastic–perfectly plastic model. The differences become most apparent near the plastified hotspot areas, where in the enhanced model, the stress field appears more concentrated.

This observation implies that by adding nonlinear hardening and strain-history dependent changes, the way in which load is locally transferred is modified once plastic deformation develops. So, it becomes evident that the constitutive differences are not only at the level of the local stress–strain curves but also directly in the structural stress distribution.

To make it possible to investigate the mechanical response at the chosen hotspots, the stress–time and stress–strain histories are extracted from the corresponding nodes. The local responses make the comparison possible to see how the two constitutive formulations evolve once plastic deformation develops within the critical regions.

The hotspot responses show that there is a big difference in the constitutive evolution of the two material formulations after the plastic deformation phase starts.

In the basic elastic–perfectly plastic model, after yielding, the stress response stabilizes in a relatively narrow range while the local deformation keeps accumulating. This beheavier is because the constitutive formulation does not have any hardening evolution, so the local response keeps moving towards a saturated stress state during continued loading.

The improved constitutive formulation through the non-linear kinematic hardening, isotropic hardening, viscoplasticity, and strain-history dependent behavior, predicts stress changes continuing over deformation.

The local constitutive response evolves differently depending on the local deformation level and loading history even though all the chosen locations are in plastified regions. The enhanced constitutive model shows these differences more clearly than the basic formulation, which means it has a stronger sensitivity to local de-formation history within plastifying regions.

5.2.3 Strain-Range dependent response at different hotspots

According to stress-strain response, the basic elastic-perfect plastic demonstrates a large local strain accumulation after yielding while the stress evolution slowly limits to a relatively narrow saturated range. This is a perfect plasticity feature, where no further hardening evolution occurs after yield has developed. Therefore, the main deformation mode after that is the accumulation of plastic strains.

On the other hand, the improved constitutive model indicates stress that keeps evolving with rising local strain. The addition of isotropic hardening, kinematic hardening, visco-plasticity, and strain-history dependence leads to local increase in material resistance when subjected to plastic deformation. Consequently, the enhanced model reaches higher stress states and at the same time it limits excessive local strain accumulation at the hotspot.

The stress-time response analysis shows that the improved constitutive model maintains a higher stress level after yielding than the basic model. This implies that the enhanced model maintains higher local stress levels and it also modifies the local stress redistribution behavior during plastic deformation.

Overall, the results demonstrate that the constitutive formulation strongly influences the local mechanical response at hotspot regions. While the basic elastic–perfectly plastic model progressively drives the response toward stress saturation, the enhanced formulation preserves a stronger sensitivity to local deformation his-tory and produces a more differentiated evolution of local stress and strain fields.

In order to deepen the investigation on how history of local deformation affects constitutive behavior, the stresses and strains extracted from the particular hotspot locations are listed in Table 3. By comparing these, it is possible to quantitatively analyse the differences between the basic and enhanced constitutive formulations respond to different local deformation levels within plastifying regions.

Table 7 Comparison of stress and strain in the base model and the enhanced model for two different nodes

Hotspot Node	Base model S. Mises	Base Model LE11	Enhanced model S. Mises	Enhanced Model Lle11
4467125	240 < S < 250	0.0025 < LE11 < 0.0099	280 < S < 340	0.0017< LE11< 0.006
5709746	~250	0.0006 < LE11< 0.0012	250 < S < 350	0.00018 < LE11 < 0.0007

According to Table 7, different local strain levels at the selected hotspot locations could be seen in both constitutive formulations. However, in the basic elastic-perfectly plastic model, while the local deformation varies, the stress response re-mains within a relatively limited range. In contrast, significantly different stress evolution is predicted in the enhanced constitutive formulation depending on the local strain history. This behavior shows that the evolution of the effective yield surface evolves continuously through isotropic and kinematic hardening mechanisms. This, in turn, allows the local constitutive response to remain dependent on the deformation history which was experienced previously during continued plastic deformation.

5.2.4 Local plastic strain evolution

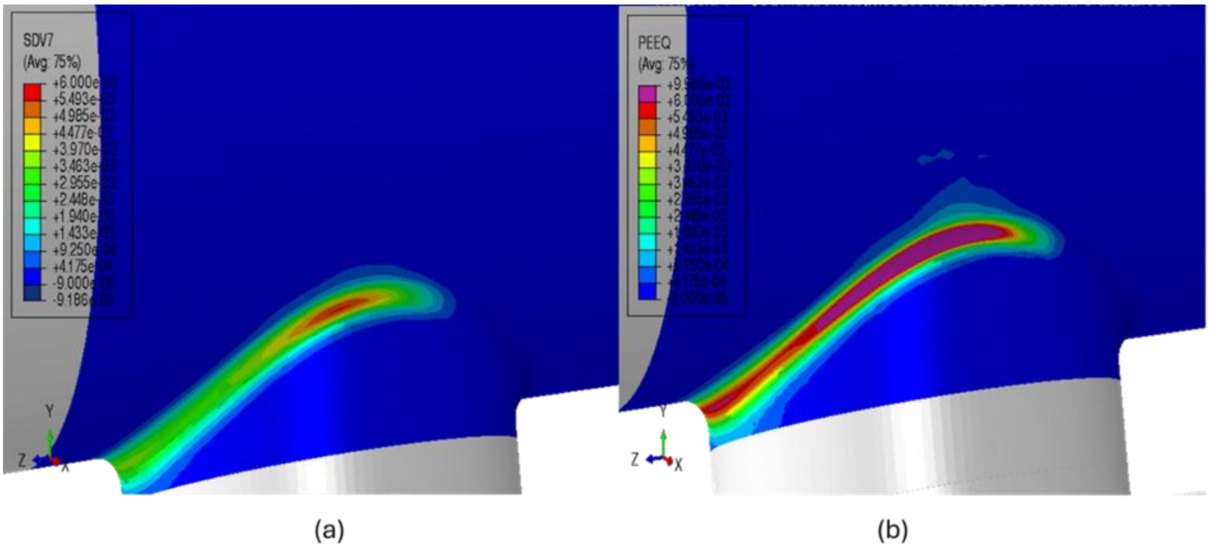

Figure 30 Comparison of accumulated plastic strain distribution predicted by (a) the enhanced constitutive model (SDV7), and (b) the basic elastic–perfectly plastic model (PEEQ)

According to figure 30, Both constitutive formulations identify localized plastic de-formation in the critical hotspot region. However, the basic elastic–perfectly plastic model shows clear higher levels of accumulated plastic strain compared to the enhanced constitutive formulation.

This behavior is consistent with constitutive behavior of the basic formulation since there is no hardening evolution after yielding, the extra deformation is mainly accommodated through the plastic strain accumulation, while the stress response progressively approaches saturation.

Enhanced constitutive formulation, on the other hand, increases material resistance during deformation by nonlinear kinematic hardening, isotropic hardening, viscoplasticity, and strain-history dependent constitutive evolution. Consequently, the enhanced model not only restricts the extreme local plastic strain accumulation but also supports a continuously changing stress response during further loading.

5.2.5 Local plastic strain evolution at hotspots

To evaluate the history of plastic deformation further at the chosen hotspot points, the accumulated plastic strain was plotted against time. The normal Abaqus PEEQ output was used for the basic model, while for the enhanced Z-mat material model, SDV7 was used since it represents accumulated plastic strain. Looking at plastic strain-time plot, it reveals that the basic elastic–perfectly plastic model develops higher accumulated plastic strain at the investigated hotspots. This is in line with the fact that there is no hardening evolution in the basic model, where continued loading after yielding is mainly accommodated through additional plastic strain accumulation. On the other hand, the enhanced constitutive model shows lower accumulated plastic strain after the same loading history. When the evolution of isotropic and kinematic hardening continues, the local material resistance increases and therefore it limits excessive plastic strain accumulation at the hotspot.

This difference is confirmed by stress–plastic strain response. In the basic model, the stress response tends to approach a saturated level while plastic strain increases continuously. In the enhanced model, when stress evolves, the accumulated plastic strain increases, which indicates that the local material resistance remains active during plastic deformation.

According to figure 30, these results show that in the enhanced constitutive model not only the stress distribution, but also the local plastic deformation history is modified, which is directly relevant to fatigue-critical hotspot behavior.

5.2.6 Relevant Interpretation

The comparisons presented in the previous section show that the choice of constitutive model highly affects the predicted mechanical behavior in the critical hotspots. While both models identify the same critical areas in the manifold, once plasticity occurs, the local stress levels, stress redistribution behavior, and constitutive response differ substantially.

In the one hand, in the basic elastic–perfectly plastic model, once a region yields, the hotspot areas might display very similar stress states. On the other hand, the enhanced material model continues to preserve the effect of the local deformation history through continuous hardening, which results in different stress levels.

From an engineering perspective, these differences are highly important since local stress range, mean stress, and constitutive state evolution are the attributes that fatigue critical parameters are directly linked to in structures that are cyclically loaded. Therefore, the enhanced constitutive model provides a rich resolution of the local stress in highly deformed regions. Although fatigue is not studied in this thesis, the results of changing the material model have high effects on mean stress and consequently the fatigue analysis.

5.3 Limitations of the Present Study

Even though the proposed constitutive model was able to adequately simulate the cyclic behavior of AISI 316L and showed enhanced predictive ability compared to the simple elastic-perfectly plastic model formulation, there are still some limitations that need to be addressed.

First, the calibration methodology was based on strain-controlled experimental results from the literature. As such, the determined material parameters are tied to the experimental conditions and could potentially need adjustment if applied to different loading paths, temperatures, or materials.

Secondly, the calibration was done by employing a one-dimensional constitutive model only. Although such a simplification significantly reduced the computational cost and made the identification of parameters easier, the calibration phase excluded the direct incorporation of multiaxial loading effects.

Thirdly, the finite element model was cantered on a particular gas manifold component submodel. Hence, the numerical outcomes of this paper are not intended to be extended to all stainless-steel parts in the absence of further validations.

Finally, the present research was limited to the cyclic behaviour at room temperature. Temperature-dependent material properties along with thermo-mechanical coupling were not considered and would likely influence the cyclic behavior.

Despite these limitations, the study not only highlights the feasibility of the implementation of an advanced strain-amplitude-dependent constitutive model within finite element frameworks but also this study recalls its potential advantages for engineering issues addressing cyclic plasticity.

5.4 Industrial and Engineering Implications

The outcomes of this research indicate that the selection of the correct material model for constitutive behavior can have a major impact on the forecasted local stress and strain fields in components prone to fatigue. better strain-amplitude-sensitive constitutive model aims to capture the cyclic material behavior more realistically than a standard elastic-perfectly plastic model.

Such enhanced prediction features can support the effective fatigue evaluation in problematic spots for engineering purposes. Taking the gas manifold design as an example, an accurate description of cyclic hardening and stress changes in the material will allow the engineers to locate vulnerable areas more precisely, carry out structural integrity evaluations at a higher level of confidence, and lessen the margin of error in the fatigue life estimations.

Furthermore, the introduced method for calibration offers the possibility of utilizing sophisticated constitutive models in finite element modelling with parameters derived from experiments. By doing so, this technique potentially decreases dependence on a large number of physical experiments and assists in the design and validation stages of the product lifecycle in a more streamlined manner.

6 Conclusion

6.1 Summary of Findings

This thesis was mainly focused on constitutive modelling of cyclic plasticity behavior characterized by nonlinear hardening evolution, history-dependent response, and Norton viscoplasticity in AISI 316L stainless steel. In this research constitutive model implementation, parameter calibration, Finite Element implementation and validation against experimental cyclic data were combined to assess the ability of advanced material modelling approaches for reproducing complex cyclic deformation behavior of this material. The data used in this study were from graphically available results for limited number of strain amplitudes in literature and all subsequent analyses were done by using the reconstructed datasets.

The research showed that perfect plastic material fails to capture the cyclic behavior of AISI 316L when it is subjected to repeated loading conditions. In the experiments, the nonlinear cyclic changes were hardening, cyclic softening, and resharpening (while in this study the interested behavior was saturated stress level after the first hardening), as well as strain amplitude dependent hardening. These characteristics were not sufficiently simulated by using simplified elastic–perfectly plastic models.

To address these limitations, a viscoplastic constitutive framework based on the combined isotropic–kinematic hardening and strain amplitude hardening was implemented and studied. Special focus was on the nonlinear hardening parameters and how they affect the evolution of stress, hysteresis loops, and strain amplitude dependent hardening. The findings indicated that the framework was able to model several keys experimentally observed cyclic features, such as the evolution of stress amplitude and the mechanical response dependent on loading history over repeated loading cycles.

The parameter calibration was done, and physical constraints were imposed. The optimizer was implemented in the way that the cost function was relative error. The relative error of the best fit for the first cycle and the last cycle was 0.001. The method illustrated a high dependence of cyclic response on interaction of isotropic hardening, kinematic hardening, viscoplasticity, and strain amplitude dependent hardening parameters. The presented parameter analyses further explained how different sets of parameters affect stabilized cyclic behavior, giving more understanding of the physical role of the different parts of the constitutive framework.

Moreover, the developed numerical scheme was evaluated by making a comparison with reference numerical solutions and finite element results. The solver verification outcomes showed good agreement with benchmark data which, in turn, validated the stability and reliability of the implementation.

The finite element analyses verified the usability of the constitutive model for cyclic loading situations in engineering applications where stress redistribution and the effects of load history are significant. Since local cyclic stress and strain fields are strongly effective on fatigue damage, the proposed framework can provide a more reliable basis for fatigue assessment in finite element simulations where the components are subjected to repeated loading.

Overall, this study emphasizes the need to account for strain amplitude dependent hardening constitutive mechanisms in the cyclic plasticity modelling of AISI 316L stain-less steel. Findings show that advanced viscoplastic formulations provide a more physically meaningful description of cyclic deformation behavior than the simplified constitutive methods, especially in conditions where the material is subjected to repeated plastic loading and changing stress histories.

Finally, this research illustrates that to have a reliable constitutive modelling of cyclic plasticity, not only it is necessary to have precise constitutive equations, but also the calibration should be done precisely to ensure that the numerical operations run smoothly and maintain that the implementing strategies are always consistent. Therefore, the implemented framework leads to an improved capability of prediction in cyclic finite element simulations with considering practical applicability in engineering analysis.

6.2 Future Research Directions

There are multiple opportunities that could be explored in future research. Firstly, the calibration procedure can be developed to consider multiaxial loading situations and paths of non-proportional loading. Secondly, the material behaviour under changes of temperature could be added for a better representation of the operating conditions of marine engines.

In subsequent investigations, researchers can explore different hardening laws formulation as well as additional strain-amplitude-dependent-hardening mechanisms to enhance the accuracy of cyclic modelling. Also, the same approach could be done for other materials that are widely used in industrial applications.

Finally, the presented modelling scheme has the potential to be directed towards a wider range of structural parts and loading cases so that the change in fatigue estimation and the results of structural integrity analysis can be measured.

References

Abdel-Karim, M., & Ohno, N. (2000). Kinematic hardening model suitable for ratchetting with steady-state. *International Journal of Plasticity*, *16*(3–4), 225–240. https://doi.org/10.1016/S0749-6419(99)00052-2

Armstrong, P. J., & Federick, C. O. (1966). *A mathematical representation of the multiaxial bauschinger effect*.

ASM handbook:P roperties and selection: Iron, Steels, and High-Performance Alloys: 1´. (1990). ASM International.

Bari, S., & Hassan, T. (2000). Anatomy of coupled constitutive models for ratcheting simulation. *International Journal of Plasticity*, *16*(3–4), 381–409. https://doi.org/10.1016/S0749-6419(99)00059-5

Besson, J., Cailletaud, G., Chaboche, J.-L., & Forest, S. (2009). *Non-Linear Mechanics of Materials*. Springer.

Chaboche, J. L. (1989). Constitutive equations for cyclic plasticity and cyclic viscoplasticity. *International Journal of Plasticity*, *5*(3), 247–302. https://doi.org/10.1016/0749-6419(89)90015-6

Chaboche, J. L. (2008). A review of some plasticity and viscoplasticity constitutive theories. *International Journal of Plasticity*, *24*(10), 1642–1693. https://doi.org/10.1016/j.ijplas.2008.03.009

Davis. (1994). *Stainless steels*.

Dowling. (2013). *Mechanical behavior of materials*.

Dunne, F. P. E., & Petrinic, N. (2005). *Introduction to Computational Plasticity*. Oxford University Press.

Facheris, G., & Janssens, K. G. F. (2014). An internal variable dependent constitutive cyclic plastic material description including ratcheting calibrated for AISI 316L. *Computational Materials Science*, *87*, 160–171. https://doi.org/10.1016/j.commatsci.2014.02.026

Fatemi, A. (1998). *Cumulative Fatigue Damage and Life Prediction Theories: A Survey of the State of the Art for Homogeneous Materials*. *20*(1), 9–34. https://doi.org/10.1016/S0142-1123(97)00081-9

Frederick, C. O., & Armstrong, P. J. (2007). A mathematical representation of the multiaxial Bauschinger effect. *Materials at High Temperatures*, *24*(1), 1–26. https://doi.org/10.3184/096034007X207589

Hill, R. (1950). *The mathematical theory of plasticity*.

Jiang, & Sehitoglu. (1996). *Modling of cyclic ratchening plasticity*.

Kovach, & Redmond. (2009). *Fatigue behavior of Austenitic stainless steels*.

Krempl, E. (2001). *On the Importance of Considering Rate Dependence in Modeling the Inelastic Behavior of Materials*. *5*, 167–188.

Lemaitre, J., & Chaboche, J. L. (2012a). *Mechanics of solid materials*. Cambridge University Press. https://doi.org/10.1017/CBO9781139167970

Lemaitre, J., & Chaboche, J. L. (2012b). *Mechanics of solid materials*. https://doi.org/https://doi.org/10.1017/CBO9781139167970 (Original work published Cambridge University Press)

Lippold, J. C., & Damian, J. K. (2005). *Welding Metallurgy and Weldability of Stainless Steels*. Wiley.

McDowell, D. L. (1995). *Stress State Dependence of Cyclic Ratchetting Behavior of Two Rail Steels*. *11*(4), 397–421.

Mises, R. von. (1913). *Mechanik der festen Körper im plastisch-deformablen Zustand*. 582–592.

Mughrabi, H. (2002). *Specific Features and Mechanisms of Fatigue in the Ultrahigh-Cycle Regime*. *24*(12), 1283–1294. https://doi.org/10.1016/S0142-1123(02)00092-2

Ohno, N. (1982). *A Constitutive Model of Cyclic Plasticity with a Nonhardening Strain Region*. *49*(4), 721–727.

Ohno, N., & Wang, J. (1993). *Kinematic Hardening Rules with Critical State of Dynamic Recovery, Part I: Formulation and Basic Features for Ratchetting Behavior*. *9*(3), 357–390. https://doi.org/10.1016/0749-6419(93)90042-O

Pelegatti, M., Lanzutti, A., Salvati, E., Srnec Novak, J., De Bona, F., & Benasciutti, D. (2021). Cyclic Plasticity and Low Cycle Fatigue of an AISI 316L Stainless Steel: Experimental Evaluation of Material Parameters for Durability Design. *Materials*, *14*(13), 3588. https://doi.org/10.3390/ma14133588

Perzyna, P. (1966). *Fundamental problems in viscoplasticity*.

Pham, M. S., Holdsworth, S. R., Janssens, K. G. F., & Mazza, E. (2013a). Cyclic deformation response of AISI 316L at room temperature: Mechanical behaviour, microstructural evolution, physically-based evolutionary constitutive modelling. *International Journal of Plasticity*, *47*, 143–164. https://doi.org/10.1016/j.ijplas.2013.01.017

Pham, M. S., Holdsworth, S. R., Janssens, K. G. F., & Mazza, E. (2013b). Cyclic deformation response of AISI 316L at room temperature: Mechanical behaviour, microstructural evolution, physically-based evolutionary constitutive modelling. *International Journal of Plasticity*, *47*, 143–164. https://doi.org/10.1016/j.ijplas.2013.01.017

Polák, J., Obrtlík, K., & Hájek, M. (1994). CYCLIC PLASTICITY IN TYPE 316L AUSTENITIC STAINLESS STEEL. *Fatigue & Fracture of Engineering Materials & Structures*, *17*(7), 773–782. https://doi.org/10.1111/j.1460-2695.1994.tb00808.x

Polak, & Man. (2016). *Behavior of AISI 316L stainless steel*.

Sedriks, A. J. (1996). *Corrosion of Stainless Steels* (2nd ed.).

Simo, J. C., & Hughes, T. J. R. (1998). In *Computational inelasticity*.

Socie, D. F., & Marquis, G. B. (2000). *Multiaxial Fatigue*. Society of Automative Engineers (SAE).

Stephens, Fatemi, & Stephens & Fuchs. (2001). *Metal fatigue in engineering*.

Voce, E. (1948). *Relationship between stress and strain for homogeneous deformation*.

WebPlotDigitizer. (n.d.). [Computer software]. Retrieved https://plotdigitizer.com/app

Zhou, J., Sun, Z., Kanouté, P., & Retraint, D. (2018a). Experimental analysis and constitutive modelling of cyclic behaviour of 316L steels including hardening/softening and strain range memory effect in LCF regime. *International Journal of Plasticity*, *107*, 54–78. https://doi.org/10.1016/j.ijplas.2018.03.013

Zhou, J., Sun, Z., Kanouté, P., & Retraint, D. (2018b). Experimental analysis and constitutive modelling of cyclic behaviour of 316L steels including hardening/softening and strain range memory effect in LCF regime. *International Journal of Plasticity*, *107*, 54–78. https://doi.org/10.1016/j.ijplas.2018.03.013

Z-set Material Model Manual: Memory Behavior. (n.d.). Z-set Software. Retrieved http://zset-software.com/wordpress/wp-content/uploads/manuals/html/z_mat_manual/Behavior/Memory.html#index-0